Original Article

MOLECULAR METABOLISM

Independent activation of CREB3L2 by glucose fills a regulatory gap in mouse β-cells by co-ordinating insulin biosynthesis with secretory granule formation

Nancy Sue [1], Le May Thai [1], Atsushi Saito [2], Cierra K. Boyer [3], Ashleigh M. Fordham [1], Chenxu Yan [1], Aimee Davenport [1], Jiang Tao [1], Mohammed Bensellam [1], James Cantley [1,5], Yan-Chuan Shi [1,4], Samuel B. Stephens [3], Kazunori Imaizumi [2], Trevor J. Biden [1,4,*]

ABSTRACT

Objective: Although individual steps have been characterized, there is little understanding of the overall process whereby glucose co-ordinates the biosynthesis of insulin with its export out of the endoplasmic reticulum (ER) and incorporation into insulin secretory granules (ISGs). Here we investigate a role for the transcription factor CREB3L2 in this context.

Methods: MIN6 cells and mouse islets were analysed by immunoblotting after treatment with glucose, fatty acids, thapsigargin and various inhibitors. Knockdown of CREB3L2 was achieved using si or sh constructs by transfection, or viral delivery. *In vivo* metabolic phenotyping was conducted after deletion of CREB3L2 in β-cells of adult mice using Ins1-CreER^{+}. Islets were isolated for RNAseq and assays of glucose-stimulated insulin secretion (GSIS). Trafficking was monitored in islet monolayers using a GFP-tagged proinsulin construct that allows for synchronised release from the ER.

Results: With a K_m ≈3.5 mM, glucose rapidly ($T_{1/2}$ 0.9 h) increased full length (FL) CREB3L2 followed by a slower rise ($T_{1/2}$ 2.5 h) in its transcriptionally-active cleavage product, P60 CREB3L2. Glucose stimulation repressed the ER stress marker, CHOP, and this was partially reverted by knockdown of CREB3L2. Activation of CREB3L2 by glucose was not due to ER stress, however, but a combination of O-GlcNAcylation, which impaired proteasomal degradation of FL-CREB3L2, and mTORC1 stimulation, which enhanced its conversion to P60. cAMP generation also activated CREB3L2, but independently of glucose. Deletion of CREB3L2 inhibited GSIS *ex vivo* and, following a high-fat diet (HFD), impaired glucose tolerance and insulin secretion *in vivo*. RNAseq revealed that CREB3L2 regulated genes controlling trafficking to-and-from the Golgi, as well as a broader cohort associated with β-cell compensation during a HFD. Although post-Golgi trafficking appeared intact, knockdown of CREB3L2 impaired the generation of both nascent ISGs and proinsulin condensates in the Golgi, implying a defect in ER export of proinsulin and/or its processing in the Golgi.

Conclusion: The stimulation of CREB3L2 by glucose defines a novel, rapid and direct mechanism for co-ordinating the synthesis, packaging and storage of insulin, thereby minimizing ER overload and optimizing β-cell function under conditions of high secretory demand. Upregulation of CREB3L2 also potentially contributes to the benefits of GLP1 agonism and might in itself constitute a novel means of treating β-cell failure.

Keywords Pancreatic β-cell; Insulin biosynthesis; Insulin secretion; O-GlcNAcylation; ER stress; ER-to-Golgi trafficking

[1]Garvan Institute of Medical Research, 384 Victoria St, Darlinghurst, NSW 2010, Australia [2]Department of Biochemistry, Institute of Biomedical and Health Sciences, Hiroshima University, Hiroshima, Japan [3]Fraternal Order of Eagles Diabetes Research Center, Department of Internal Medicine, University of Iowa, Iowa City, IA 52246, USA [4]St Vincent's Clinical School, Faculty of Medicine, The University of New South Wales, Sydney, Australia

[5] Current address: Division of Systems Medicine, University of Dundee, Ninewells Hospital & Medical School, Dundee, DD1 9SY, United Kingdom.

*Corresponding author. Garvan Institute of Medical Research, 384 Victoria St, Darlinghurst, NSW 2010, Australia. E-mail: t.biden@garvan.org.au (T.J. Biden).

Abbreviations: AICAR, 5-aminoimidazole-4-carboxamide ribonucleoside; AMPK, AMP activated kinase; CHOP, C/EBP homologous protein; DEG, differentially expressed gene; ER, endoplasmic reticulum; FA, fatty acid; FL, full-length; GSIS, glucose-stimulated insulin secretion; GTT, glucose tolerance test; HBP, hexosamine biosynthesis pathway; HFD, high fat diet; HGDMEM, high glucose Dulbecco's modified Eagles medium; ISG, insulin secretory granule; ISR, integrated stress response; ITT, insulin tolerance test; KRHB, Krebs Ringer Hepes Buffer; KO, knockout; LGDMEM, low glucose Dulbecco's modified Eagles medium; mTOR, mammalian target of rapamycin; OGT, O-GlcNAc transferase; O-GlcNAc, O-linked β-N-acetylglucosamine; P-60, N-terminal cleavage product of CREB3L2; PERK, PKR-like ER kinase; RUSH, Retention Using Selective Hooks; T2D, Type 2 diabetes; UPR, unfolded protein response; WT, wild-type

Received June 13, 2023 • Revision received November 22, 2023 • Accepted November 23, 2023 • Available online 25 November 2023

https://doi.org/10.1016/j.molmet.2023.101845

1. INTRODUCTION

The regulation of insulin biosynthesis by glucose is controlled independently of insulin secretion, but is needed to replete and maintain the pool of ISGs that are available for exocytosis [1—4]. Activation of proinsulin gene expression is important over the longer term, but translational control predominates during the first 4 h of glucose stimulation [1,5]. This is specific to proinsulin and a few dozen other ISG components [1,5] thereby optimizing the processing and folding of mature insulin [1—4]. Not to be confused with the distal trafficking of exocytosis, this proximal pathway constitutes vesicular export from the endoplasmic reticulum (ER) to Golgi, as well as the post-Golgi formation and maturation of ISGs.

Insulin biosynthesis exhibits a dose dependency that is left-shifted relative to that of GSIS, and is not activated by other nutrient secretagogues such as fatty acids (FAs) [1,5]. It also requires the metabolism of glucose but not the gating of Ca^{2+} channels [1,5]. These differences point to alternative mechanisms for glucose sensing, potentially involving nutrient-regulated protein kinases such as mTORC1 and AMP-activated kinase (AMPK) [6,7]. Another means of nutrient-sensing involves the conversion of glucose to N-acetylglucosamine (GlcNAc) via the hexosamine biosynthesis pathway (HBP), an offshoot of the early steps of glycolysis. GlcNAc is incorporated into protein via O-glycosidic linkages in a reaction catalysed by the O-GlcNAc transferase (OGT) enzyme. O-GlcNAcylation is implicated in the regulation of proinsulin gene expression by glucose, and is beneficial for GSIS, but its characterization in β-cells remains incomplete [8,9].

ER stress arises when the rate of export of secretory protein from the ER fails to match that of biosynthesis, thereby triggering the unfolded protein response (UPR) [10—12]. Initially, this transcriptional response is beneficial; it stalls protein synthesis, and upregulates the expression of protein chaperones and genes that control the exit from the ER of proteins, which are destined for either degradation, or trafficking to the Golgi Apparatus. If this adaptive UPR fails to resolve ER stress, however, apoptosis is triggered, partly mediated by upregulation of the transcription factor CHOP [10—12]. The UPR is transduced by 3 signalling pathways that link the ER and nucleus. These comprise: the protein kinase PERK; the transcription factor ATF6; and the splicing regulator IRE1. Activation of PERK promotes the phosphorylation EIF2a, thereby inhibiting the translation of proteins including proinsulin [10—12]. This nexus is also targeted by protein kinases activated independently of ER stress, in a process known as the integrated stress response (ISR) [13]. This also induces CHOP. The primary substrate of IRE1 is the transcription factor, XBP1. Its spliced form (XBP1s), constitutes the best documented arm of the UPR for regulating protein export between the ER and Golgi [14,15].

CREB3L2 is another transcription factor with relevance to ER-to-Golgi trafficking, and is also activated in response to ER stress [16]. It forms part of family that includes other CREB3L isoforms, as well as ATF6 and SREBPs, all of which exist in precursor forms as transmembrane proteins in the ER [16]. Following stimulation these are trafficked to the Golgi where proteolytic cleavage releases an active, N-terminal fragment that translocates to the nucleus to regulate transcription. For CREB3L2, release from the ER does not seem to involve interacting proteins as in the case for ATF6 and SREBPs [16]. Rather, ER stress appears to inhibit the otherwise robust clearance of the full-length (FL), precursor CREB3L2, such that more is available for transfer and activation in the Golgi [17,18]. CREB3L2 regulates genes of the early secretory pathway, most notably the Sec23 and Sec24 isoforms that are critical components of the COPII complex [19,20]. This drives formation of budding vesicles on the surface of the ER that package cargo destined for export to the Golgi [21]. CREB3L2 also encodes a broad suite of other genes including components of the classical UPR, as well as more cell-specific programs [19,20]. However, little is known of the function of CREB3L2 in β-cells apart from a single report of a positive role in GSIS [22].

2. MATERIALS AND METHODS

2.1. Animals

Approval for all studies was provided by the Garvan/St Vincent's Hospital Animal Ethics Committee. Mice on a C57Bl6/J background were bred at Australian BioResources (Moss Vale, Australia) and then maintained on site for experimental work. Male animals were used, except were indicated for some studies with isolated islets. They had *ad libitum* access to food and water, and were housed with 12 h light/dark cycles under pathogen free conditions. Feed comprised either standard chow (10.88 kJ/g; 8% fat, 21% protein, and 71% carbohydrate) or a HFD (19.67 kJ/g; 45% fat, 20% protein, 35% carbohydrate). Deletion of CREB3L2 was achieved by floxing Exon 2 in the mouse Creb3l2 gene, using standard techniques. For selective deletion of CREB3L2 in adult beta cells, the floxed Creb3l2 (*Creb3l2*$^{f/f}$) animals were mated with either *Pdx1-CreER*$^{+}$ [23] or Ins1-CreER^{+} mice [24]. In addition to knockout groups *Creb3l2*$^{f/f}$ cre^{+} (KO), we employed multiple controls comprising *Creb3l2*$^{f/f}$ cre^{-} (flox); *Creb3l2*$^{f/+}$ cre^{+} (het); and *Creb3l2*$^{+/+}$ cre^{+} (cre). For deletion 8-week-old mice were orally gavaged a total of 3 times at two-day intervals with 4 mg tamoxifen (dissolved in 100 ml of 10% ethanol/sunflower oil. HFDs were started the following week, for an additional 8 weeks. Genotyping was undertaken using the following primers [20]: forward 5'-ctgcagtggtcagatggacagag-3' (WT and KO); reverse 5'-ccagcaggactgcaaatggctg-3' (WT) and 5'-cttgacgagttcttctgagg-3'.

2.2. Metabolic studies

Glucose (GTT) and insulin tolerance tests (ITT) were performed on male mice fasted for 6 h. For GTTs, glucose was administered orally at a dose of 3 g/kg body weight [25]. For ITTs, insulin was injected intraperitoneally (i.p.) at a dose of 0.75 U/kg body weight [26]. Blood glucose levels were sampled an Accu-check Performa glucose monitor. Blood samples were also taken during GTTs for insulin assays using a mouse Ultra Sensitive ELISA (Crystal Chem, IL, USA). Total, lean and fat mass were analysed by EchoMRI.

2.3. Islet isolation

Islets were isolated as previously described [25,26] using ductal perfusion of Liberase T-flex (Roche Diagnostics, Australia) or Collagenase V (Sigma Aldrich), and purified on Ficoll-Paque gradients (GE Healthcare, Chalfont St Giles, UK) [27]. For assay of GSIS, islets were maintained overnight in tissue culture using RPMI 1640 media (11 mM glucose) supplemented with 10% FCS, 0.2 mM glutamine, 10 mM HEPES, 50 units/ml of penicillin and 50 μg/ml streptomycin. Islets from each mouse were used in at least 4 replicates of 5 islets per treatment condition in Krebs Ringer HEPES buffer (KRHB) containing 0.1% BSA. After 1 h preincubation in KRBH (2.8 mM glucose) at 37 °C, islets were washed and stimulated for a further hour with either 2.8 mM or 20 mM glucose. Insulin released into the media, or retained in the islet pellet, was quantified using a radioimmunoassay (Merck Millipore, Bayswater, Victoria, Australia) or FRET-based Insulin Ultra-Sensitive Assay (Cisbio, Codolet, France). For immunoblotting, the total isolate from each mouse was cultured and preincubated as above, then stimulated for 1—4 h in KRBH at 2.8 mM or 20 mM glucose.

2.4. Cell culture and assays

MIN6 insulinoma cells [28] (passages 30–37) were passaged in DMEM containing 25 mM glucose (HGDMEM), supplemented with 10% FCS, 10 mM HEPES, 50 units/ml of penicillin and 50 μg/ml streptomycin. Cells were seeded 4×10^5 cells per well in 12-well plates, or at 1×10^6 in 6-well plates. Unless otherwise stated, all media was from Thermo-Fisher, to which inhibitors and other compounds as sourced from Sigma Aldrich were added where appropriate. For chronic treatments, cells were exposed to thapsigargin (24 h), or either oleate or palmitate (both 0.4 mM final pre-coupled to 0.92 g BSA/100 ml), or BSA control in DMEM containing 5 mM glucose (LGDMEM) for 48 h [29]. Media was replaced after 24 h and cells maintained for a further 48 h. For overexpression and lentiviral knockdown studies, cells were treated in HGDMEM and then switched after 24 h to LGDMEM with BSA and FAs (as above) for a further 48 h prior to harvest. Where indicated, the plasmids pcDNA(3.1+)-Flag-mouse BBF2H7 (FL-CREB3L2), or Flag-BBF2H7-376 (P60 N-terminus) [18] were transfected using Nanojuice transfection reagent (Merck Millipore) as previously described [30]. For short term (1–6 h) glucose stimulations, cells were usually switched to LGDMEM 24 h prior to study, then pre-treated for 1 h in KRBH (1 or 2.8 mM glucose) before stimulation for 1 or 4 h with 10 or 20 mM glucose as indicated. However, for si transfections, time course studies, and treatments with leucine, rapamycin and 5-Aminoimidazole-4-carboxamide ribonucleotide (AICAR), cells were maintained in HGDMEM, but then preincubated in serum free DMEM (2.8 mM glucose and 0.1% BSA) for 4 h. Cells were stimulated with glucose ± inhibitors for times as indicated. Studies of si knockdown were as previously described [31] using cells transfected in OptiMEM medium (Thermo Fisher) with Dharmacon ONTARGETplus SMARTpool siRNA directed towards CREB3L2 or scrambled control using Dharmafect3 reagent (Dharmacon, Pittsburg, PA, USA). Apoptosis was measured using the Cell Death Detection ELISA Plus Kit (Roche Diagnostics).

2.5. Viruses

SureSilencing short hairpin (sh) plasmids for knocking down CREB3L2 were purchased from Qiagen and subcloned into pRRL-PGK lentiviral transfer vector for transformation of TOP10 competent cells (Thermo Fisher). After maxi-prepping, plasmids corresponding to Creb3l2 sh2 and sh4, as well as GFP and scrambled (scr) controls, were transfected along with packaging plasmids into HEK293FT cells (Thermo Fisher) by Ca-PO_4-DNA precipitation. Viral particles were harvested and concentrated by centrifugation using Amicon 0.45 mm filters (Sigma Aldrich). For adenoviruses, a plasmid containing a U6 promoter-driven Creb3L2 shRNA targeting mouse sequence in an adenoviral backbone co-expressing mCherry was obtained from Vector Builder. Non-targeting control (shSAFE) was provided by the University of Iowa Viral Vector Core Facility. AdRIP-proCpepRUSH has been described elsewhere [32]. Recombinant adenoviruses were generated in HEK293 cells and purified by cesium chloride gradient. All sequences were verified by the Iowa Institute of Human Genetics, University of Iowa.

2.6. Gene expression analysis

Following extraction of RNA from MIN6 cells using RNeasy mini kits (Qiagen), cDNA was synthesised using Omniscript (Qiagen). Gene expression was analysed by qRT-PCR using Taqman probes (Applied Biosystems, Mulgrave, Victoria, Australia) and an HT-7900 machine. mRNA expression of all genes was normalised to gene expression of HPRT1 or TBP [27]. The following probes were used: Creb3l1, Mm00496405_ml; Creb3l2, Mm00618366_ml; Creb3l3, Mm00520279_ml; Creb3l4, Mm00518698_ml; Atf6, Mm01295319_ml; Hprt1, Mm01545399_ml; Tbp, Mm01277042_ml.

2.7. RNA sequencing

Mice were fed a HFD for 8 weeks, and RNA was extracted from islets of a single mouse per replicate using RLT buffer (Qiagen). After purification using RNAeasy Kits, quantification and integrity analysis (RIN > 9.3) was undertaken at the Garvan Molecular Genetics Core Facility using the Agilent 4200 TapeStation System. Replicates consisted of 4 het controls, and 5 KOs. 500 ng of RNA was used for library preparation using the KAPA mRNA HyperPrep Kit. Following library QC using a DNA 1000 chip in the LabChip GX Touch, each sample was diluted to 2 nM and was sequenced using the NovaSeq 6000 platform at a depth of 30 million reads per sample. Data files were quality checked, (FastQC), trimmed (Trimgalore), aligned to the reference mouse genome using the Illumina BaseSpace Dragen RNA-seq Pipeline, and tabulated as transcripts per million counts (TPM). Differentially expressed genes were identified using R and further analysed using DESeq2. Significantly altered genes were further investigated using platforms available on the Enrichr portal 35 (GO, Reactome and Jensen compartments) as well as KEGG.

2.8. Immunoblotting

Protein was extracted from islets or MIN6 cells with radioimmunoassay precipitation buffer (ThermoFisher) and quantified using bicinchoninic acid assay (ThermoFisher). 15–30 μg protein was resolved on a pre-cast 10% or 12% NuPAGE Bis-Tris gel (ThermoFisher), and transferred to a PVDF membrane as previously described [26,30]. These were blocked for 1 h in 5% skim-milk, and probed at 4 °C overnight with antibodies purchased from: Sigma–Aldrich, Creb3l2 (HPA015068), beta actin (A5441); tubulin, (T6074), SEC23a, (ABC424); ThermoFisher, O-linked N-Acetylglucosamine (MAI-072); Santa Cruz, Pan 14-3-3 (sc-1657); and Cell Signalling Technology, CHOP (L63F7) (CST2895), phospho-EIF2a (Ser51) (CST 9721), phospho-mTOR (Ser2481) (CST 2974), phospho-PERK (Thr980) (CST 3179), phospho-ACC (ser79) (CST 3661), and cleaved caspase-3 (CST 9662). After chemiluminescent detection, quantification was carried out using ImageJ (NIH, Bethesda, MA, USA). All quantitative data was corrected for loading, as determined in the same gels using antibodies against beta actin, Pan 14-3-3, or tubulin.

2.9. Fluorescence microscopy and imaging

Pools of islets were transduced with ~$1–5 \times 10^8$ IFU/mL adenovirus for 18 h in standard RPMI medium, switched to RPM1 with 7.5 mM glucose, and assayed 72–96 h post-treatment. This results in approximately 50% transgene expression in the islet. Adenoviral knockdown was achieved using CREB3L2 shRNA or control, coinfected with an mCherry reporter identify targeted cells. To address proinsulin trafficking we exploited the Retention Using Selective Hooks (RUSH) system, whereby proinsulin is retained in the ER until specifically released into the secretory pathway by addition of biotin [32]. RUSH requires co-expression of constructs encoding ER-targeted streptavidin, and in our case, a β-cell-directed reporter, AdRIP-ProCpepRUSH [32]. The latter incorporates GFP and streptavidin binding peptide into the C-peptide region of preproinsulin. Isolated islets expressing proCpepRUSH (AdRIP) were gently dispersed into monolayer sheets using Accutase (Sigma–Aldrich) and plated onto HTB9 coated coverslips [32]. To initiate proCpepRUSH trafficking, biotin was added to a final concentration of 200 μM in the culture media and cells fixed in 10 % neutral-buffered formalin at 180 min [32]. For immunostaining, permeabilized cells were incubated overnight with an antibody raised against GM130 (mouse, BD Transduction 610823). Highly cross-adsorbed fluorescent conjugated secondary antibody (whole IgG, donkey anti-mouse AlexaFluor 647; Jackson ImmunoResearch) was

used for detection. Cells were counterstained with DAPI and mounted using Fluorosave (Calbiochem). shRNA expressing cells were identified by mCherry reporter expression. For granule counting and distance measures, images were captured on a Leica SP8 confocal microscope using a HC PL APO CS2 63×/1.40 oil objective with 3× zoom as z-stacks (5 per set, 0.3 μm step, 0.88 μm optical section) and deconvolved (Huygen's Professional). Total ISGs were quantified using Imaris (Bitplane) from spot-rendered RUSH positive granules defined as 150–300 nm objects and normalized to the total number of mCherry positive, proCpepRUSH-labeled cells. Granule distance measurements from the Golgi were determined using a distance transformation module in Imaris (Bitplane) from spot-rendered proCpepRUSH-positive granules (150–300 nm) and surface rendering of the Golgi identified through GM130 immunostaining. Granule distances were binned as indicated and expressed as a percentage of the total to normalize between cells and conditions [32,33].

3. QUANTIFICATION AND STATISTICS ANALYSIS

Results are usually presented showing individual data points, mean and standard error of the mean (SEM). All statistical analyses were conducted using Prism (version 9) software (GraphPad) using tests as indicated in the figure legends.

4. RESULTS

4.1. CREB3L2 is abundant in β-cells but plays little role during lipotoxic ER stress

CREB3L2 was by far the most highly expressed of the CREB3-like/OASIS family of transcription factors in both MIN6 cells (Figure 1A), and mouse islets (Suppl. Figure 1a), as determined by RT-PCR and RNAseq respectively. Indeed, its abundance was similar to that of the UPR mediator, ATF6, under baselines conditions (Figure 1A and Suppl. Figure 1a) although, as expected, the latter was further increased by thapsigargin, a strong inducer of ER stress (Figure 1A). At the protein level, both the full-length (FL) precursor, and the cleaved active fragment of CREB3L2 were readily detected (Suppl. Figure 1b). The latter ran consistently at around 50 kDa in MIN6 cells, as well as mouse islets. This was true even when overexpressed, although in this case a slower migrating band was also detected (Suppl. Figure 1b). This size is somewhat smaller than reported for other cell types, possibly due to differences in glycosylation [18], but for consistency with the prior literature we will refer to the cleaved, active fragment as P60.

To determine whether ER stress impacts on CREB3L2 protein expression in β-cells, we exploited our lipotoxicity model, whereby MIN6 cells are exposed to moderately elevated levels of BSA-coupled

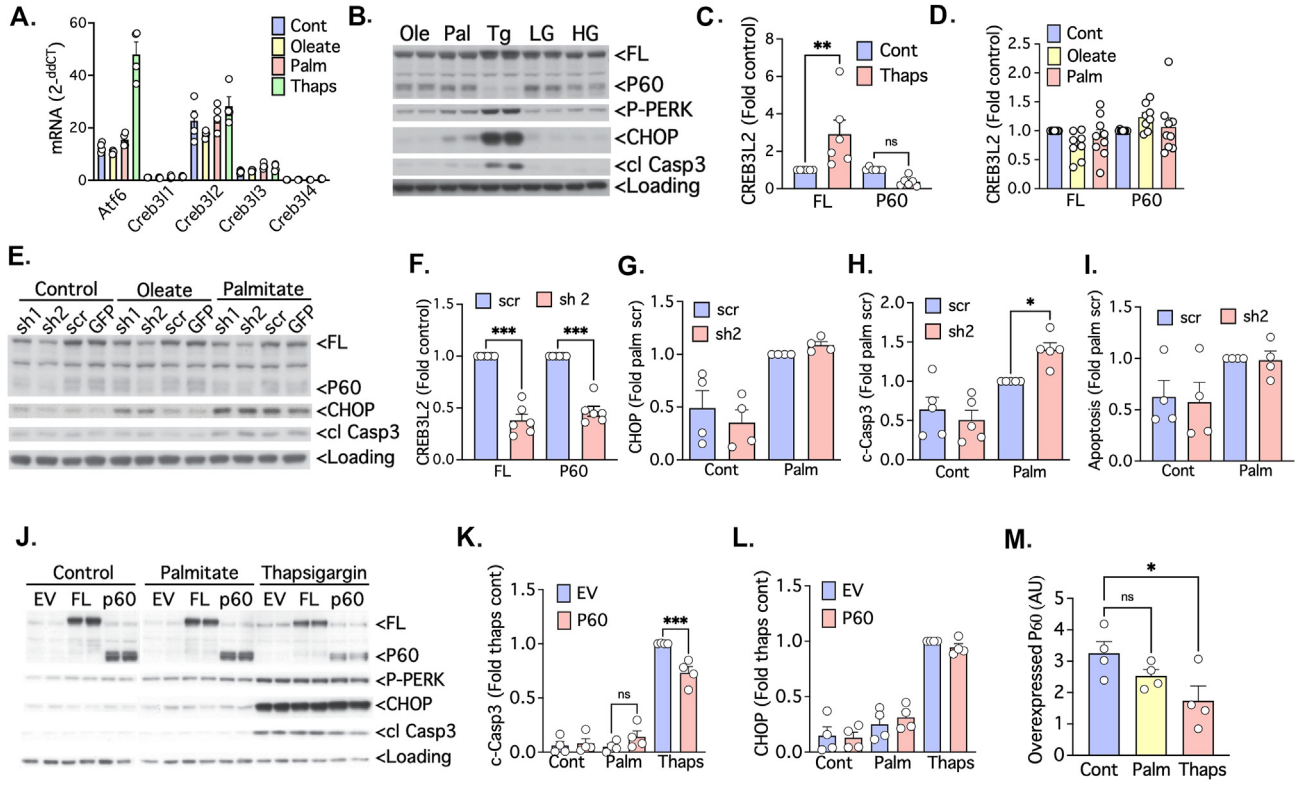

Figure 1: CREB3L2 is not a major interactor with lipotoxic ER stress. MIN6 cells were pretreated with BSA control (0.92 g/100 ml), or oleate (0.4 mM) or palmitate (0.4 mM) for 48 h, or thapsigargin (300 nM) for 24 h in LGDMEM. (A), qPCR was performed on RNA extracts to quantify expression of gene transcripts as indicated. (B–M), Cells were lysed and subjected to immunoblotting, and bands corresponding to the identified proteins quantified by densitometry. (B), Representative images. (B–D), effects of thapsigargin (B), FAs (C) or glucose (D) on CREB3L2 species. (E–I), cells were co-treated during FA preincubation with lentiviral constructs encoding GFP control, scramble control (scr) or two different short hairpin (sh2 & 4) constructs directed against Creb3l2. (E), Representative images. Quantification of effects of control or sh2 Creb3l2, on either FL-CREB3L2 or P60 themselves (F), CHOP (G), cleaved caspase 3 (H). (I), Apoptosis assay of cells treated as in (E–H). (J–M), cells were transfected with plasmids encoding GFP control, FL-Creb3l2 or P60 for 48 h, and co-treated for the last 24 h with palmitate or thapsigargin. (J), Representative images. (K–L), quantification of effect of P60 overexpression on (K) cleaved caspase 3 or (L) CHOP. (M), quantification of overexpressed P60 after treatment with palmitate or thapsigargin. *$p < 0.05$, **$p < 0.01$, ***$p < 0.001$ as indicated, using 1-way ANOVA with Holm-Sidak multiple comparisons test.

palmitate (3:1 molar ratio) [29] for 48 h at 5 mM glucose. This and similar models recapitulate multiple features of the β-cell failure associated with T2D and, most importantly, predicted the relevance of ER stress as an underlying etiology [10,13,34–36]. We first confirmed that markers of ER stress (CHOP and phospho-PERK) and apoptosis (cleaved caspase-3) were increased by thapsigargin and palmitate, but not the unsaturated FA, oleate (Figure 1B). However, in contrast to thapsigargin (Figure 1B, C) neither FA altered CREB3L2 proteins (Figure 1B, D). We further established that transient increases in CREB3L2 expression were not revealed by shorter term exposure to FAs (Suppl. Figure 1c–e).

Although not further activated by palmitate, CREB3L2 proteins were detectable in even unstimulated β-cells (Figure 1B), so we questioned whether this constitutive activity might still be important in the context of lipotoxicity. Lentiviral knockdown of CREB3L2 was undertaken using 2 different constructs, of which sh2 was more effective (Figure 1E) and used for quantification of the depletion of both protein species (Figure 1E, F). However, CHOP expression was unaltered by loss of CREB3L2 in palmitate-treated cells (Figure 1E, G), and although there was an enhancement of caspase-3 cleavage under these conditions (Figure 1H), this was not reflected in actual β-cell apoptosis (Figure 1I). Conversely overexpression of FL-CREB3L2 did not impact on markers, regardless of how ER stress was induced (Figure 1J). Moreover, the overexpression of the active P60 form of CREB3L2, modestly protected against caspase-3 cleavage in response to thapsigargin, but not palmitate (Figure 1J, K). Enhancing P60 did not alter CHOP levels under any conditions (Figure 1L). An additional (and surprising) finding was that the accumulation of P60 was actually suppressed by thapsigargin (Figure 1M). This was more apparent with overexpressed P60 than for the endogenous protein (Figure 1B), most probably because the latter is able to be repleted by conversion from the FL precursor. Although not pursued further, this suggests that the degradation of P60 is increased after strong and prolonged ER stress.

4.2. Glucose is a major regulator of CREB3L2 activation in β-cells

We next assessed whether increasing the ambient glucose concentration from 5 mM to 25 mM might unmask an effect of FAs on CREB3L2 activation, but this was not the case (Figure 2A–C). Surprisingly, however, 48 h exposure to high glucose alone enhanced accumulation of the active P60 fragment, but not FL-CREB3L2 (Figure 2A–C). Moreover, the ER stress marker CHOP was reduced under these conditions (Figure 2A, D), consistent with its known suppression by glucose [37–39]. We reasoned that this might be mediated by the concomitant activation of CREB3L2. Indeed, knocking down this transcription factor selectively increased CHOP levels, from the lower baseline observed in the presence of high glucose (Figure 2E, F). As a control, we also confirmed that loss of CREB3L2 reduced expression of the ER-to-Golgi trafficking protein, Sec23a, as it does in other cell types [19,20] (Figure 2E, F). Collectively these results suggest that glucose is a more important activator of CREB3L2 than lipotoxic ER stress in β-cells, and conversely this potentially helps preempt the ER stress that would otherwise be triggered by glucose-stimulated protein synthesis.

MIN6 cells faithfully mirror primary mouse islets in terms of dose-dependency and other key features of both GSIS and insulin biosynthesis [1,5,29,40], so were used for further elaboration of the glucose response. Time-course studies established that the increase in P60 ($T_{1/2}$ 2.5 h) was considerably delayed relative to that of the FL species ($T_{1/2}$ 0.9 h) (Figure 2G). Comparable results were obtained using mouse islets (Suppl Figure 2a). We next determined that the elevations of FL-CREB3L2 and P60 displayed similar concentration dependencies for glucose, with IC50s of approximately 3.4 mM (Figure 2H), which are comparable to that for proinsulin biosynthesis [5]. This was broadly confirmed in mouse islets, where we additionally showed that CREB3L2, especially the active P60 form, was further increased by elevations of glucose above the fed euglycemic level of 7 mM (Figure 2I). Furthermore, expression of FL-CREB3L2, but not P60, was reduced in islets from mice fed a prior HFD. Even so, 4-h stimulation of mouse islets with glucose significantly augmented both species regardless of diet (Figure 2J, K).

4.3. O-GlcNAcylation and mTORC1 co-operate to mediate CREB3L2 activation by glucose

To address mechanisms underlying the glucose response, we first focused on the 1 h timepoint at which only FL-CREB3L2 is elevated, since this species is the major site of regulation in other cell types [17,18]. We found no requirement for the gating of Ca^{2+} channels, nor the release of insulin into the medium, since uncoupling these processes from glucose metabolism by treatment with the K^+ channel opener, diazoxide, did not alter the accumulation of FL-CREB3L2 (Figure 3A, B). There was, however, a requirement for oxidative metabolism because both CREB3L2 species were dramatically diminished by hypoxia (Suppl Figure 2b). Conversely, elevation of cAMP, using the pharmacological activator forskolin, was sufficient to increase the precursor protein (Figure 3A, C). Notably, these increases were additive to those of glucose, indicating that the latter works independently of cAMP generation. Similar results were obtained using Exenatide, an agonist of the GLP1 receptor that also raises cAMP (Figure 3A, D).

In other cell types the turnover of the precursor protein is not simply determined by its conversion to P60, but more importantly by its rapid degradation by the proteasome [18]. Indeed, both forms of CREB3L2 were greatly augmented in β-cells by the proteasomal inhibitor MG132. Importantly, this was non-additive to the glucose response (Figure 3E, F), indicating that glucose does not promote the upstream synthesis of CREB3L2, in which case a synergistic response should have been observed with MG132. Notably, an abundant, slower-migrating band of FL-CREB3L2 (and to lesser extent P60) was also revealed in the presence of MG132 (Figure 3E). As elucidated in other cell types [18], this most probably represents a non or lesser-glycosylated form, which is not usually observed due to its rapid degradation [17]. Blockade of ongoing protein synthesis using cycloheximide greatly reduced the accumulation of FL-CREB3L2 (Figure 3G, H), as expected for a protein that is turned over quickly. Importantly, this was not observed for P60 (Figure 3G, I). Collectively these results suggest that, like MG132, glucose inhibits the degradation of FL-CREB3L2, facilitating its conversion to the active (and more stable) P60 fragment.

To test whether O-GlcNAcylation might link glucose metabolism with the stabilization of CREB3L2 proteins, we focused on a longer (4 h) stimulation with glucose, which allows for elevation of both CREB3L2 species (Figure 4A). Using an antibody capable of detecting O-GlcNAc incorporated in proteins, we firstly confirmed that this was reduced by the OGT inhibitor, OSMI1 [41] (Suppl Figure 3a). Conversely, modest OGT-dependent increases were observed in some bands due to 4 h glucose exposure (Suppl Figure 3a), as quantified for one example (band X) (Suppl Figure 3b). More importantly, OSMI1 blocked the glucose-stimulated increments in FL-CREB3L2 (partially) and P60 (virtually completely) (Figure 4A, B). Notably, OSMI1 also promoted the appearance of a slower migrating form of FL-CREB3L2 (Figure 4A). However, this band was less apparent than that observed with MG132 treatment (Figure 3E), suggesting that it is highly susceptible to

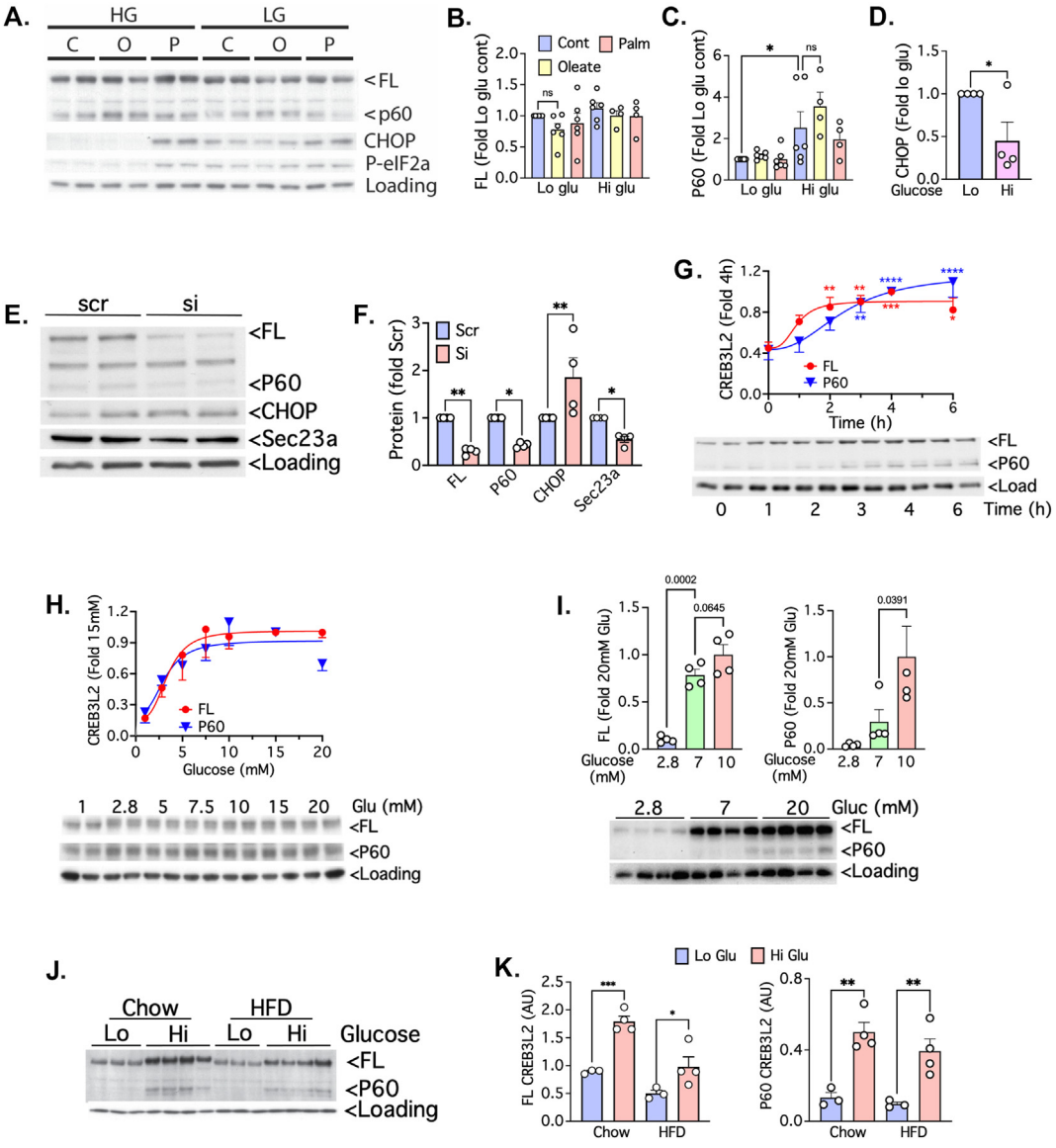

Figure 2: Activation of CREB3L2 contributes to reduced ER stress during acute glucose treatment. MIN6 cells (A—H) or isolated mouse islets (I—K) were lysed and subjected to immunoblotting, and bands corresponding to CREB3L2 species or CHOP quantified by densitometry. (A—D), Effects of chronic glucose exposure. Cells were treated for 48 h in LGDMEM (Lo) or HGDMDM (Hi). (A), Representative images. (B—D), Quantification of FL-CREB3L2 (B), P60 (C) and CHOP (D). (E—F), Loss of CREB3L2 augments CHOP and reduces Sec23a at high glucose. Cells were transfected with scrambled (scr) controls or pooled Creb3l2 si in HGDMEM for 72 h, then preincubated in serum free LGDMEM for 4 h, and then stimulated for 3 h in DMEM containing 20 mM glucose (E), Representative image. (F), Quantification. (G), Time course of glucose stimulated CREB3L2 accumulation. Cells were treated as in (E—F) except that the incubation period was 0—6 h as indicated and responses quantified relative to the 4 h response ($n = 6$). (H), Glucose dose dependency of CREB3L2 accumulation. Cells were pretreated for 1 h in KRBH (2.8 mM glucose) and then stimulated in KRBH with glucose as indicated for 1—2 h (FL-CREB3L2) or 2—4 h (P60) and quantified relative to the 15 mM response ($n = 3$—6). The representative image is for a 2 h stimulation. (I), Glucose activates CREB3L2 in mouse islets. After overnight culture RPMI, islets were pre-incubated in KRBH containing 2.8 mM glucose, and then stimulated as indicated. (J, K) Modulation of CREB3L2 expression in mouse islets isolated from mice maintained on a prior 8-week chow or HFD. Islets were pretreated for 2 h in RPMI media at 2.8 mM glucose, and then incubated for 4 h in RPMI media with glucose at 2.8 mM (Lo) or 20 mM (Hi). (J) Representative images. (K) Quantification. Indicated comparisons are by one way ANOVA with Holm-Sidak multiple comparisons test (C, F, G, K); or unpaired t-test (D). Also shown are comparisons versus respective 0-time control by 2-way ANOVA with Dunnett's multiple comparisons test (G). *$p < 0.05$, **$p < 0.01$, ***$p < 0.001$, ****$p < 0.0001$.

degradation by the proteasome. We next tested the impact of blocking substrate provision to OGT, rather than directly disrupting the enzyme itself. This was achieved by using azaserine to inhibit GFPT1, the rate-limiting step of the HBP [41]. The effects on CREB3L2 were broadly similar to those of OSMI1, although the inhibition was less pronounced and a slower-migrating band was not detected (Figure 4D, E). Finally, we assessed the converse intervention of blocking the removal of GlcNAc from proteins, by using Thiamet G as an inhibitor of the O-GlcNAcylase (OGA) [41]. This promoted a global increase in O-GlcNAcylation that was apparent even at low glucose, and was more pronounced than that due to high glucose alone (Suppl Figure 3a). Both CREB3L2 species were modestly increased by Thiamet G, but only in the presence of high glucose to maintain flux through the HBP (Figure 4A, C). This implies that the rate of removal of O-GlcNAc from

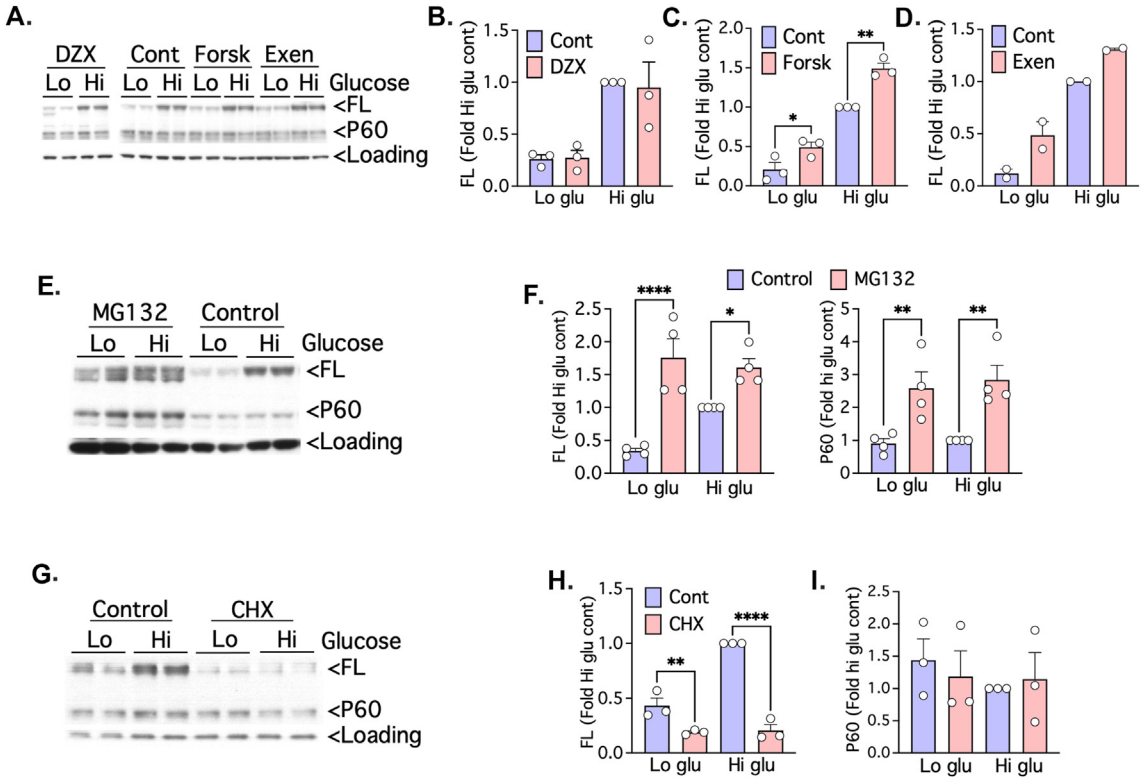

Figure 3: Accumulation of FL-CREB3L2 due to glucose is non additive to proteasomal inhibition, additive to cAMP generation, and independent of Ca^{2+} flux. MIN6 cells were pretreated in KRBH for 1 h at 1 mM glucose (A—F) or 2.8 mM glucose (G—I) and then stimulated for 1 h in KRBH containing 1 mM or 10 mM glucose (A—F) or 2.8 mM and 20 mM glucose (G—I). Cells were (were lysed and subjected to immunoblotting, and bands corresponding to CREB3L2 species quantified by densitometry. (A—D) cAMP but not Ca^{2+} regulates FL-CREB3L2. (A) Representative image. (B—D) Quantification of effects of co-stimulation in the presence of (B) 0.1 mM diazoxide, (C) 10 μM forskolin, and (D) 10 nM Exenatide. (E, F) Glucose and proteasomal inhibition act non-additively on FL-CREB3L2 and P60. (E), Representative image, and (F) quantification of effects of co-stimulation in the presence of 1 μM MG132 on FL-CREB3L2 and P60. (G—I) FL-CREB3L2 is rapidly turned over. (G) Representative image, and quantification of effects of co-stimulation in the presence of 0.1 mM cycloheximide on (H) FL-CREB3L2 and (I) P60. *$p < 0.05$, **$p < 0.01$, ****$p < 0.0001$ as indicated, using 1-way ANOVA with Holm-Sidak multiple comparisons test.

CREB3L2 is relatively low, and that glucose acts predominately to enhance its incorporation. Alternatively, O-GlcNAcylation of the FL precursor is necessary but not sufficient for the activation of CREB3L2 by glucose.

To identify other potential regulators, we assessed the involvement of nutrient-sensing protein kinases. Notably, the mTORC1 inhibitor rapamycin completely abolished the glucose-stimulated increase in P60, but was without effect on the precursor (Figure 4F, G). On the other hand, activation of mTOR with leucine, was not sufficient to augment either CREB3L2 species. Nor were they altered by AICAR (Figure 4F, G), which abolishes the repression of AMPK due to high glucose [7]. Controls confirmed that these interventions were acting as expected on AMPK (phospho-ACC) and mTORC1 (phospho-mTORC1 (Suppl Figure 3c). These findings suggest that mTOR activation by glucose complements O-GlcNAcylation, by selectively enhancing the formation of P60 and/or promoting its stabilization.

4.4. Loss of CREB3L2 impairs GSIS *ex vivo*, and *in vivo* following a HFD

For further investigation of the function of CREB3L2 we generated mice in which Exon 2 of the gene was floxed. These were mated with Ins1-CreER^{+} animals [24], to facilitate conditional deletion of CREB3L2 in adult β-cells following treatment with tamoxifen. Deletion efficiency was confirmed by immunoblotting (Figure 5A). We next performed oral GTTs (oGTTs) on chow-fed mice, but observed no effect of CREB3L2 ablation on the profiles of either glucose or insulin (Figure 5B, C), regardless of whether Flox, Cre or Het controls were used (Figure 5B, C). When islets were isolated from these animals, however, and maintained overnight at 10 mM glucose to augment CREB3L2 expression, GSIS was found to be impaired from the KO islets (Figure 5D). This was not accompanied by any depletion of insulin content (Figure 5E). Similar results were obtained using islets from mice in which deletion of CREB3L2 was driven by inducible expression of another tamoxifen-regulated Cre cassette, Pdx1-CreER^{+} [23] (Figure 5F, G). We reasoned that a whole-body phenotype might be unmasked by the elevated excursions in blood glucose that accompany high-fat feeding. For clarity of exposition and optimisation of statistical power, we combined cre and het controls for these comparisons (Figure 5H—J), although individual control curves are also shown in Suppl. Figure 4a—c. Regardless, loss of CREB3L2 impaired both glucose tolerance and insulin secretion under these conditions (Figure 5H, I), without changing insulin tolerance (Figure 5J). Likewise, there was no alteration in overall body weight, or lean or fat mass in these animals due to CREB3L2 ablation (Suppl. Figure 4d—f).

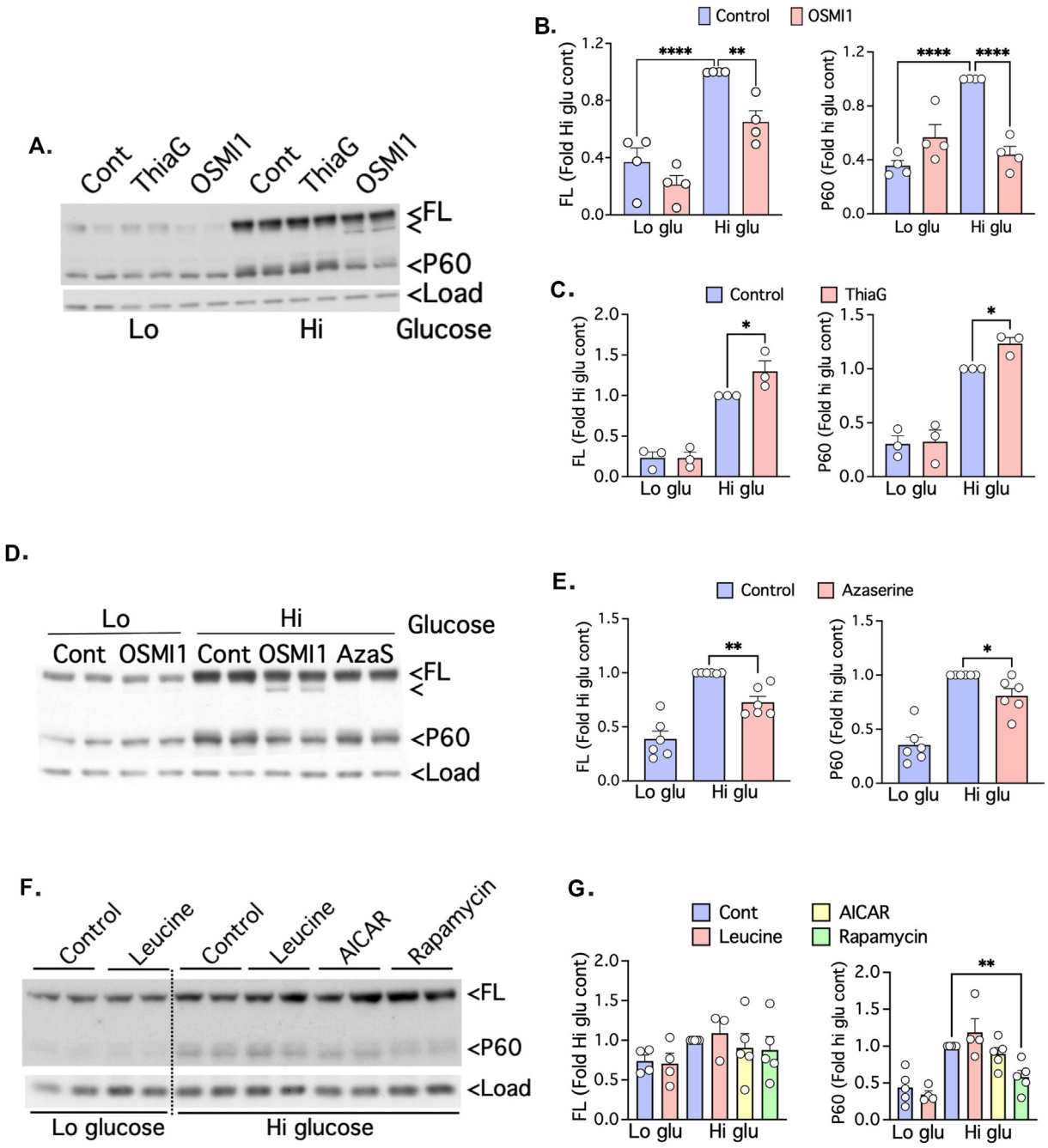

Figure 4: Roles for o-GlcNAcylation and mTORC1 respectively in the regulation of FL-CREB3L2 and P60 by glucose. MIN6 cells were pretreated in KRBH for 1 h at 2.8 mM glucose (A—E) or in serum free LGDMEM for 4 h (F, G). They were then stimulated with 2.8 mM (Lo) or 20 mM (Hi) glucose for either 4 h in KRBH (A—E) or 3 h in serum-free DMEM (F, G). Cells were (were lysed and subjected to immunoblotting, and bands corresponding to CREB3L2 species quantified by densitometry. (A—C) O-GlyNAcylation regulates CREB3L2. (A) Representative image. (B, C) Quantification of effects of co-stimulation in the presence of (B) 50 μM OSMI1 and (C) 100 μM ThiametG. (D, E) CREB3L2 activation by glucose partly depends on the HBP. (D) Representative image. (E) Quantification of effects of co-stimulation in the presence of 10 μM azaserine. (F, G) mTORC1 regulates P60 in response to glucose. (F) Representative image. (G) Quantification of effects of co-stimulation in the presence of 5 mM leucine, 2 mM AICAR, and 200 nm rapamycin. *$p < 0.05$, **$p < 0.01$, ****$p < 0.0001$ as indicated, using 1-way ANOVA with Holm-Sidak multiple comparisons test.

4.5. CREB3L2 targets genes in the early secretory pathway, as well as a subset involved in β-cell compensation

RNAseq was next employed to characterize the genes regulated in β-cells by CREB3L2 during a HFD. We identified more than 300 differentially expressed genes (DEGs) under these conditions, although fold changes were relatively modest due to a conservative strategy of comparing islets from KO versus het mice, rather than flox or cre-controls (Figure 6A, Suppl. Table 1). The great majority of genes (>200) were positively regulated by CREB3L2, of which nearly a quarter mapped to the ER and Golgi compartments, with a smaller number also associated with ISGs (Figure 6A, B, Suppl. Table 1). In particular, the early secretory pathway was highlighted by Gene

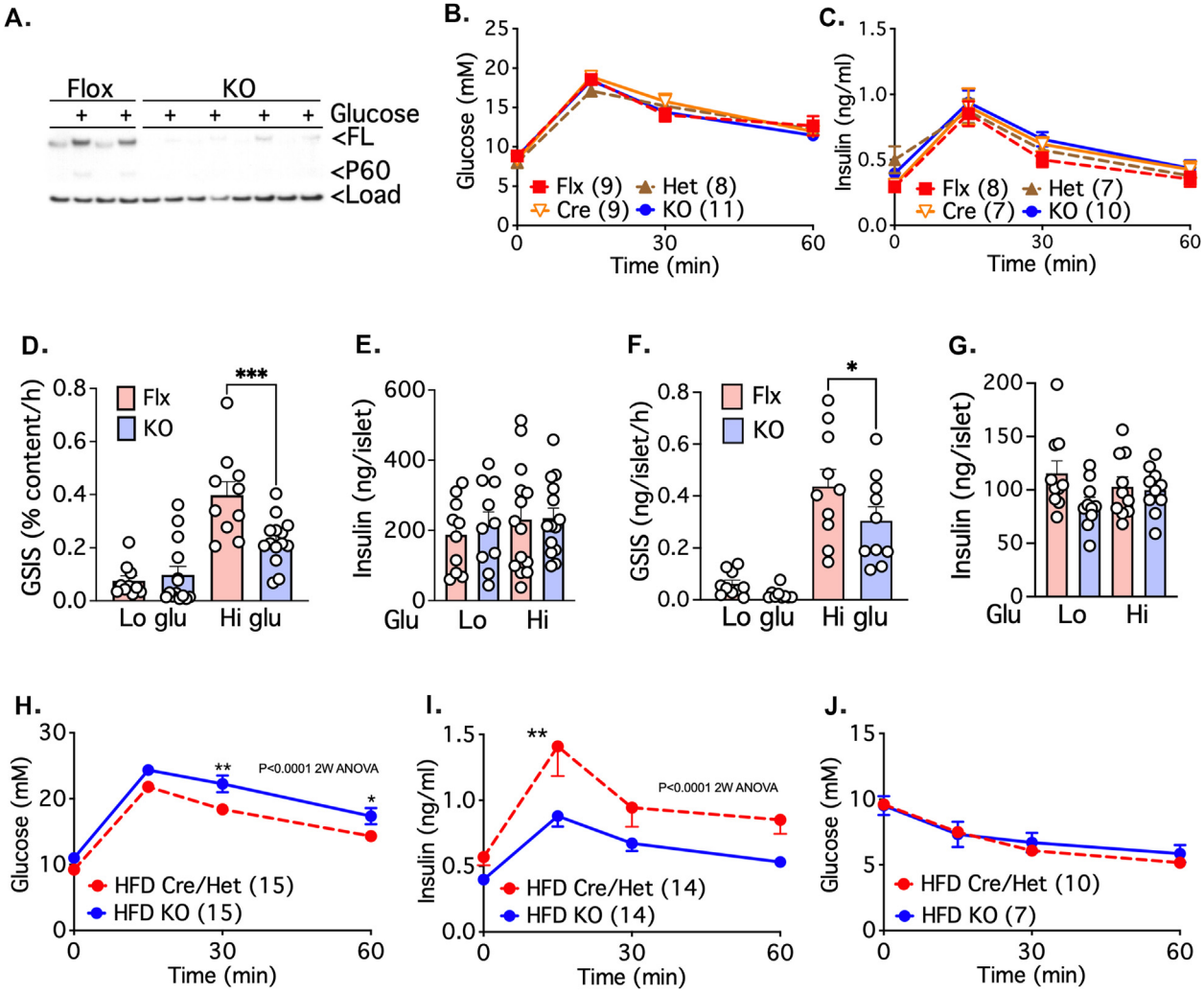

Figure 5: Deletion of CREB3L2 in adult β-cells impairs GSIS and glucose tolerance. Ins1-CreER^{+} Creb3l2$^{f/f}$ (A–E, H–J) or Pdx1-CreER^{+} Creb3l2$^{f/f}$ (F, G) KO mice, or respective controls, were orally gavaged with tamoxifen at 8-weeks of age. They were then placed on chow (B–G) or HFD (H–J) for a further 8 weeks, and subjected to *in vivo* metabolic profiling (A–C) or used for islet isolation (D–G). (A), Representative image of immunoblots of isolated islets confirming deletion of CREB3L2 species. (B, C), CREB3L2 deletion does not impact on glucose tolerance in chow-fed mice. Glucose (B) and insulin (C) excursions in Creb3l2 KO mice or controls undergoing oGTTs (n = 7–11). (D–G), *ex vivo* GSIS is impaired by CREB3L2 deletion in islets of chow-fed 16-week old KO or control mice. After overnight tissue culture in RPMI 1640 media (11 mM glucose) islets were pretreated for 1 h in KRBH containing 2.8 mM glucose, and then incubated for a further 1 h in KRBH with either 2.8 mM (Lo) or 20 mM glucose (Hi). Insulin was assayed in the medium (D, F) or in extracted islet pellets (E, G). Islets from male (F, G) or both male and female mice (D, E) were employed. (H–J), CREB3L2 deletion impairs glucose tolerance in mice on a HFD. Glucose (H) and insulin (I) excursions in Creb3l2 KO mice or controls undergoing oGTTs (n = 14–15). (J), Glucose levels in mice undergoing ipITTs (n = 7–10). Indicated comparisons are by one way ANOVA with Holm-Sidak multiple comparisons test (D, F). Also shown are comparisons of overall cre/het versus KO curves by 2-way ANOVA, with Holm-Sidak's multiple comparisons test for time points as indicated (H, I). *p < 0.05, **p < 0.01, ***p < 0.001, ****p < 0.0001.

Ontology analysis (Figure 6C, Suppl. Table 1). Strikingly, in examining the "Protein Processing in the ER" category in KEGG, we found that 7 of the 11 genes for structural components of the COPII complex, were positively controlled by CREB3L2 (Figure 6D). In contrast, there were no changes in functional genes involved in COPII cargo selection, such as Lman1, Mia3, Ctage5, Surf4, and Wsf1 [21,42–45] (Suppl. Table 1). It is also notable that only 4 genes of 86 from the Reactome UPR category (Gfpt1, Kdelr3, Arfgap1, and Sec31a) differed significantly between het and KO islets. This further validates the conclusions above that CREB3L2 and ER stress are not as strongly associated in β-cells as in other cell types. Of the Golgi-associated gene products, many function in vesicular trafficking between ER and Golgi, of which several (Copa, Copb2, Copg, Copz2) had been previously shown to be regulated by glucose [46]. There was also a smaller cohort associated with forward movement through the Golgi complex, including components relating to trafficking *per se* (Cog5, Rab33b, and Snap23) and protein glycosylation (Maged1, B4Gat1, Chst12, Slc35c1, and Slc35a2) (Suppl. Table 1). Also upregulated were genes involved in the processing of proinsulin, either directly (Pcsk1) or by transporting zinc for its stabilization (Slc30a5). Another gene of interest is Yip3f3, which was identified in a CRIPSR screen as a positive regulator of insulin content [47], and is closely related to Yipf5 (p_{adj} = 0.068), previously implicated in post-ER trafficking and neonatal diabetes [48]. Ier3ip1 encodes an ER resident protein that is also mutated in forms of neonatal diabetes, with accompanying loss of insulin content and β-cell maturation [49]. Golgi stress has also been implicated in some aspects of β-cell failure [50], and the closely related transcription factor CREB3 is a canonical marker of this

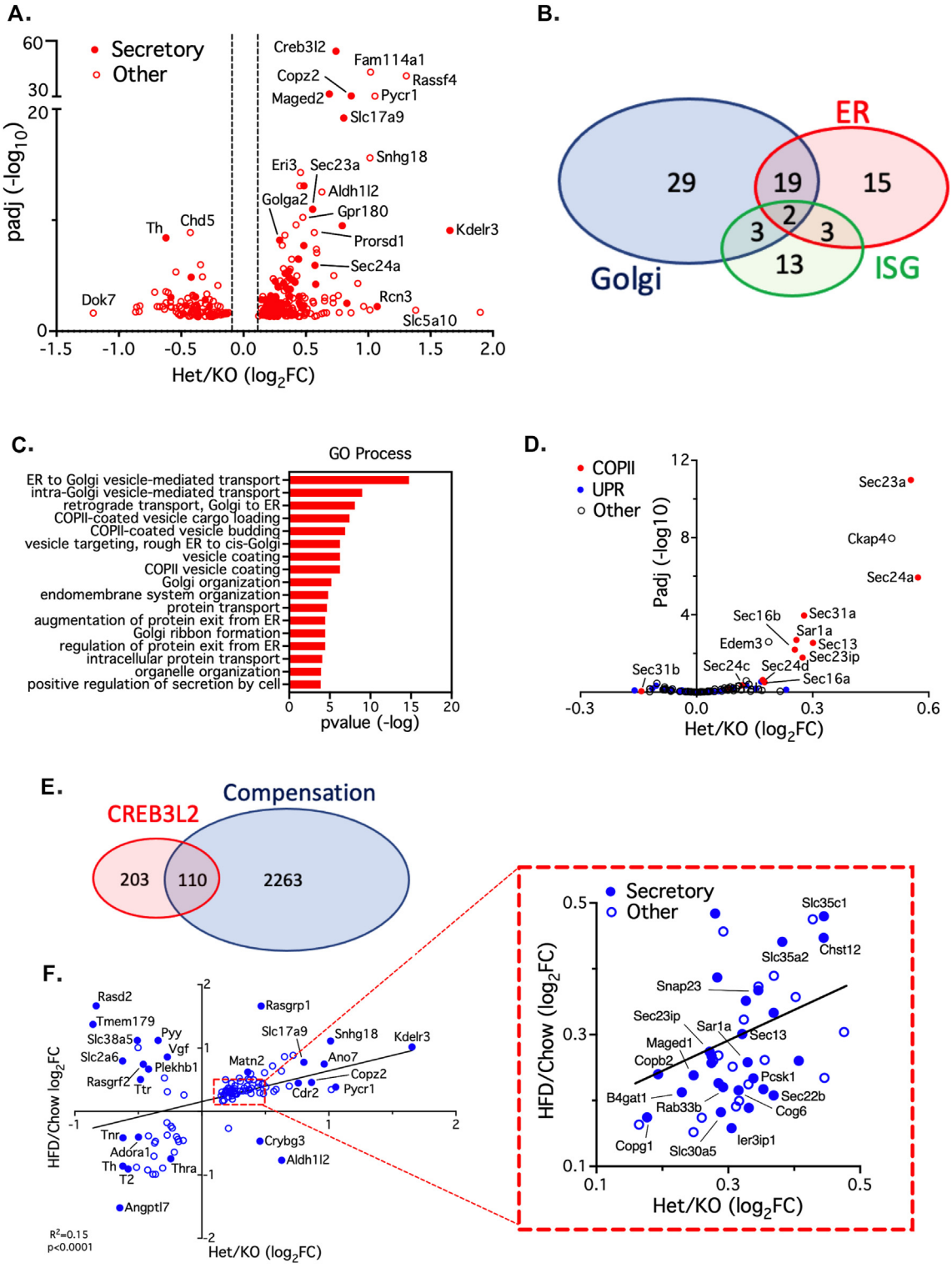

Figure 6: CREB3L2 regulates the secretory pathway and β-cell compensation. Ins1-CreER^{+} Creb3l2$^{f/f}$ (KO) and Ins1-CreER^{+} Creb3l2$^{f/+}$ (het) mice were orally gavaged with tamoxifen at 8-weeks of age, and then placed on a HFD for a further 8 weeks. RNA was extracted from islets and subjected to RNAseq. (A–F), Analyses of the ≈300 differentially expressed genes (DEGs) that differed significantly ($p_{adj} < 0.05$) between het and KO islets. (A) Volcano plot of DEGs, highlighting those mapping to secretory pathways versus others. (B), Venn diagram of DEGs that were localized to secretory pathways (Jensen Compartments) of the ≈200 that were significantly more abundant in het versus KO islets. (C), Top Gene Ontology categories of DEGs. (D), Volcano plot of all genes detected in the KEGG category "Protein Processing in the ER", highlighting COPII and UPR components. (E), Venn diagram showing overlap between DEGs due to Creb3l2 deletion and those previously associated with β-cell compensation in response to a HFD [52]. (F) Correlation of the 110 overlapping genes identified in E). Log_2 fold changes in each data set were compared by simple linear regression. $p = 0.0001$, $r^2 = 0.15$.

phenomenon. Apart from, Cog6, however, markers such as Atf3, Atf4, as well as Creb3 [50], were unaltered following deletion of CREB3L2 (Suppl. Table 1).

Upregulation of the early secretory pathway has been previously postulated as a mechanism of β-cell compensation under conditions of obesity and insulin resistance [51,52]. Indeed, more than a third of our DEGs overlapped with of minor subset of islet genes previously shown to be altered after a HFD [52] (Figure 6E). Indeed, there was a pronounced correlation between these overlapping genes (Figure 6F). Most, but not all, of these related to the early secretory pathway and Golgi function. Collectively these results strongly implicate CREB3L2 is a major regulator of β-cell compensation, of which optimizing the export of processing of secretory proteins is one important and specialized function.

4.6. CREB3L2 regulates proinsulin trafficking in the early secretory pathway

Using adenoviral CREB3L2 shRNA we first confirmed efficient gene knock-down following infection of isolated islets (Figure 7A). This was accompanied by inhibition of GSIS without alteration total insulin content (Figure 7B, C), in total agreement with the prior results using WT or CREB3L2 KO islets (Figure 5D—G). For functional validation of the RNAseq data we analysed trafficking in the early secretory pathway using the RUSH system, which allows for retention of tagged proinsulin in the ER prior to its release as a synchronized pulse in response to biotin administration. As previously shown [32], most proinsulin was incorporated into nascent ISGs by 3 h in control cells, although some was still visualized in the Golgi as puncta (Figure 7D), representing protein being condensed prior to export [53]. Knockdown of CREB3L2 markedly reduced the incorporation into nascent ISGs (Figure 7D-F), consistent with a disruption at some point in the proximal secretory pathway. As an indicator of the efficiency of post-Golgi trafficking, we measured the distribution of ISGs at various distances from the Golgi as a percentage of the overall number of labelled ISGs [32,33]. This was not altered by loss of CREB3L2, even when distances very close to the Golgi were quantified (Figure 7G). This suggests that post-Golgi export is little affected, and that the overall reduction in ISGs under these conditions is due to a major requirement for CREB3L2 further upstream in the secretory pathway. Indeed, we also observed a clear reduction in Golgi-localized proinsulin condensates due to knockdown of CREB3L2 (Figure 7D,E,H), consistent with defects in either the delivery of proinsulin to the Golgi from the ER, or delays in transit within the Golgi itself. Although further work will be required to resolve these possibilities, our current data clearly show that CREB3L2 is critical for the co-ordination of proinsulin synthesis in the ER with its packaging into nascent ISGs.

5. DISCUSSION

A major conclusion of our study is that, in addition to stimulating insulin biosynthesis and distal exocytosis, glucose also regulates intermediate steps between these two processes. This is mediated by CREB3L2, which closely aligns with insulin biosynthesis in terms of time course and dose-dependency for glucose, despite clear differences in underlying mechanisms. The repertoire of genes controlled by CREB3L2 is highly selective for protein trafficking to-and-from the Golgi, and we further showed that loss of this transcription factor disrupted incorporation of proinsulin into nascent ISGs. Thus, CREB3L2 helps co-ordinate multiple steps in early secretory pathway to help synchronise the production of proinsulin with its packaging and storage in ISGs. Critically, however, this represents a role for glucose, which is active, rapid, and not reliant on changes in the ER protein load to become manifest. This is unexpected. Based largely on results in other cell types [14,15], it had been tacitly assumed that any regulation of these steps would be mediated passively by the XBP1 arm of the UPR. However, XBP1 differs from CREB3L2 in two major ways. Firstly, its gene targets extend beyond the early secretory pathway, and include programs for lipogenesis and protein folding and degradation [14,15] that are not controlled by CREB3L2. This probably explains the more severe phenotypes reported for β-cell deletion of IRE1 [54] or XBP1 [55] as compared to that shown here for loss of CREB3L2. Secondly, there is no evidence for direct activation of XBP1 by glucose. It does promote the rapid phosphorylation of IRE1, but this is not associated with increases in XBP1s in β-cells [56]. Rather, XBP1 splicing is only triggered once unfolded protein begins to accumulate in the ER and, importantly, and there is a further lag until the spliced XBP1 protein is itself synthesized. This contrasts with the other, more rapidly developing arms of the UPR, mediated by ATF6 and PERK, which are activated directly by post-translational modifications.

The activation of CREB3L2 by glucose, and its restricted set of target genes, represents a functional specialization of the β-cell. In chondrocytes and pituitary cells, for example, genes related to the UPR, ER biogenesis, translation and amino acid metabolism are targeted in addition to those of the early secretory pathway [19,20]. Moreover, in most other cells types CREB3L2 is primarily activated as consequence of protein overload and the onset of the UPR [16,18]. Because of this, our initial focus was on lipotoxicity, a model of β-cell failure in T2D with particular relevance to ER stress [10,13,36]. However, CREB3L2 was not activated by palmitate, nor did its knockdown exacerbate the accompanying ER stress. This would be consistent our previous findings that lipotoxic ER stress in β-cells involves an impairment of ER-to-Golgi trafficking [57], secondary to lipid remodelling and depletion of ER lipid rafts [10,58,59]. This functional defect would trump any benefit of a more proximal, genetic upregulation of trafficking genes by CREB3L2. In contrast, the capacity for high glucose to induce ER stress is most likely due to its stimulation of protein synthesis, rather than any specific defect in protein folding or trafficking [37,60]. Notably, CREB3L2 was recently identified as one of several transcription factors whose nominal gene targets were upregulated in adult human β-cells, in association with increased rates of protein synthesis [61]. Thus, the co-activation of CREB3L2 by glucose would be expected to forestall this ER stress, by enhancing the transit of newly synthesised proinsulin out of the ER lumen. This would be consistent with prior findings [37—39] that the terminal ER stress marker CHOP is suppressed by glucose. We further demonstrated that CREB3L2 was partially required for that suppression. However, we did not observe a broader ER stress signature amongst the DEGs in our RNA seq analysis. On the other hand, glucose exposure was previously shown to reduce EIF2a phosphorylation [37,60,62], but analyses [37] suggested that this, and the decreases in CHOP expression, were more probably explained by modulation of the ISR rather than UPR. Thus, teasing out the precise roles of CREB3L2 in mediating the complex engagement of glucose with the UPR and ISR will require much further work, conducted under defined condition and using a more extensive suite of markers than employed here.

In response to ER stress, the accumulation of CREB3L2 is ultimately determined by the inhibition its degradation in the proteasome [17]. Glucose also appears to converge on this mechanism in β-cells, since its activation of CREB3L2 was non-additive with that of the proteasomal inhibition. Although both CREB3L2 species were augmented under these conditions, we would argue that FL-CREB3L2 is the major site of regulation for several reasons. Firstly, the increase in FL-

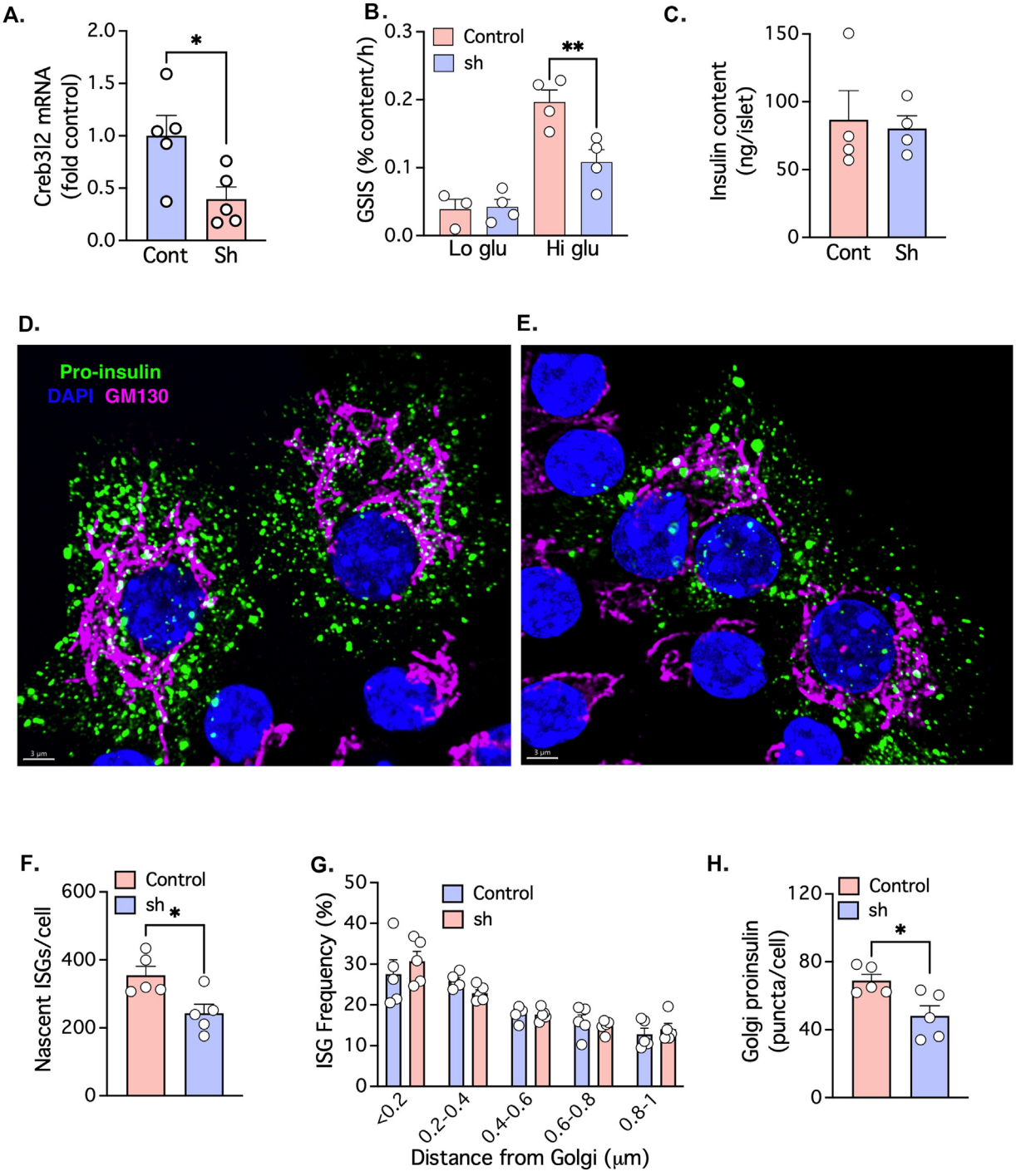

Figure 7: Knockdown of CREB3L2 in mouse β-cells impairs GSIS, nascent ISG formation, and proinsulin trafficking through the early secretory pathway. Isolated mouse islets were infected in RPMI 1640 media (11 mM glucose) with adenoviruses containing either control shRNA or Creb3L2 shRNA containing an mCherry reporter (A–H) as well as AdRIP-proCpepRUSH (D–H). (A), qPCR was performed on RNA extracts to quantify expression of Creb3l2. (B, C), GSIS is impaired by CREB3L2 knockdown. Islets were pretreated for 1 h in KRBH containing 2.5 mM glucose, and then incubated for a further 1 h in KRBH with either 2.5 mM (Lo) or 12 mM glucose (Hi). Insulin was assayed in the medium (B) or in extracted islet pellets (C). Loss of CREB3L2 impairs formation of nascent ISGs (D, E, F) and condensation of Golgi proinsulin (D, E, H), without altering the percentage distribution of labelled ISGs at indicated distances from the Golgi (D, E, G). Infected islets were dispersed on monolayers in RPMI medium containing 7.5 mM glucose, and 200 μM biotin added to initiate release of tagged proinsulin from the ER. Cells were fixed after 3 h, stained as indicated and then imaged using fluorescent microscopy. shRNA expressing cells were identified by mCherry expression. Representative images of cells treated with sh control (D), and sh CREB3L2 (E). Quantification of nascent ISGs (F), ISG percentage distance distribution from Golgi (G) and proinsulin condensates co-localized with GM130 (H). Indicated comparisons are unpaired t-test (A, C, F, H), or by one way ANOVA (B) with Holm-Sidak multiple comparisons test. *$p < 0.05$, **$p < 0.01$.

CREB3L2 clearly preceded that of P60, which is inconsistent with a direct effect of glucose on the stabilization of P60. Secondly, when translational synthesis was blocked with cycloheximide, FL-CREB3l2 was profoundly diminished whereas P60 was unaltered, suggestive a much faster degradation of the precursor protein. Thirdly, proteasomal clearance is determined by ubiquitination of the target proteins, and at least for CREB3L1, where this has been extensively studied, ubiquitin ligases are selectively recruited to areas of the FL protein that are absent in the active fragment [17]. Fourthly, we showed that CREB3L2 activation was critically dependent on glucose-regulated O-GlcNAcylation, which is broadly implicated in the control of protein ubiquitination and clearance. Specifically, inhibitors of both the proteasome and O-GlcNAcylation increased slower migrating bands of FL-CREB3L2, consistent with a non-glycosylated form that, because of its rapid degradation, would not normally be seen. Equivalent forms of P60 were much less apparent or non-existent. Collectively these findings suggest that FL-CREB3L2 is selectively stabilized by O-GlcNAcylation in response to glucose, resulting in a greater rate of conversion to P60 (Figure 7). Although it seems most likely that FL-CREB3L2 is itself a substrate for O-GlcNAcylation, until this is confirmed directly and the sites mapped in future studies, we do not exclude a role for upstream substrates that somehow stabilize FL-CREB3L2 indirectly. Regardless, our work adds to a growing appreciation of the importance of O-GlcNAcylation in β-cells. These express the highest levels of OGT in the body [9,63], and display an otherwise paradoxical diversion of some glycolytic flux toward the HBP. Indeed, generation of O-GlcNAc via the HBP was critical for the regulation of CREB3L2, although we do not rule out additional effects of glucose on the expression or activation of OGT. Notably, β-cell deletion of OGT results in a glucose-dependent augmentation of CHOP [64], to which impaired activation of CREB3L2 might contribute. However, CREB3L2 represents only one of multiple transcription factors likely to be regulated by O-GlcNACylation, and which contribute to the enhancement of insulin gene expression, and prolongation of acute secretory responsiveness, following short-term glucose exposure [8,9]. This would be consistent with our finding that CREB3L2 controls a more restricted set genes than the overall cohort previously shown to be regulated by O-GlcNAcylation [8,65].

mTORC1 is a classic stimulator of general protein biosynthesis but its role in the activation proinsulin translation by glucose is controversial and perhaps permissive [62]. We found that mTORC1 selectively enhanced accumulation of P60 but not FL-CREB3L2 in glucose-stimulated β-cells, suggestive of a different mechanism of action to O-GlcNAcylation. By analogy with its roles in regulating the activity of SREBP1c [66], mTORC1 might act to facilitate the trafficking or proteolytic cleavage of FL-CREB3L2, thereby enhancing its processing to P60. Although mTORC1 also inhibits proteasomal degradation of many proteins [67], it is harder to envisage how this would be selective for P60 versus FL-CREB3L2, especially since the latter appears to be the more obvious target for this pathway, as discussed above. Thus, O-GlcNAcylation and phosphorylation by mTORC1 seemingly act in tandem to mediate the activation of CREB3l2 by glucose (see Graphical Abstract).

Our study further showed that glucose is not the sole activator of CREB3L2 in β-cells. Forskolin, a strong inducer of cAMP, also promoted accumulation of FL-CREB3L2, but to a lesser extent than glucose. Moreover, the combination of both stimuli gave an additive response, suggestive of different underlying mechanisms. Indeed, available evidence favours a transcriptional site of action for cAMP in stimulating CREB3L2 in other cell types [68], as opposed to the post-translational mechanisms described here. We have not formally tested this possibility, but perhaps it accounts for the effects we observe with forskolin and Exenatide, and makes a small contribution to the overall response to glucose. Even so, activation of CREB3L2 (via cAMP production) should now be added to potential benefits of GLP1 agonists on β-cell function, especially in the context of their capacity to alleviate ER stress [69,70]. We also found that hypoxia markedly impaired CREB3L2 accumulation, consistent with a requirement for the mitochondrial metabolism of glucose, as previously implicated in the synthesis of ISG proteins [1–4]. Compellingly, hypoxia was previously shown to impair ER-to-Golgi trafficking in β-cells [71]. Inhibition of HIF1a was evoked as a putative explanation, based on the down-regulation of several candidate genes in the early secretory pathway [71]. However, several of these genes (Copa, Copg, and Copz2) were also identified as targets of CREB3L2 in our unbiased screen, suggestive of an alternative, or additional, mechanism.

Our study also suggests that CREB3L2 contributes to the process whereby β-cells adapt to the increased insulin demand associated with obesity and insulin resistance. In our hands, deletion of CREB3L2 impaired β-cell function specifically in obese mice on a HFD, and the DEGs identified under these conditions correlated strongly with subset previously shown to be associated with β-cell compensation [52]. As discussed above, our KO phenotype is more likely to be explained by elevations in blood glucose due to high fat feeding, rather than an effect of lipotoxicity *per se*. We do not exclude, however, that CREB3L2 might also be required to mediate the compensatory benefits of some systemic factor(s). Growth factors such as TGFβ and IGF1 are potential candidates and, indeed, both have been shown to signal via CREB3L2 in other cell types [72,73]. Regardless, and as a corollary, our elucidation of this novel role for CREB3L2 might help explain why decompensated ER stress does not develop in β-cells of animal models solely as a consequence of enhanced insulin demand, but requires a prolonged HFD [74,75]. Rather, as in human T2D [76], a separate (or overriding) defect is required, that we have previously argued is provided by a genetic susceptibility to lipotoxicity [10]. This can be phenocopied by palmitate pretreatment *in vitro*, but not normally by a HFD *in vivo* [10].

Consistent with prior *in vitro* results using INS1E cells [22] our study showed that either deletion or knockdown of CREB3L2 in mouse islets impaired GSIS, without any alteration in total insulin content. There was, however, a clear reduction in the incorporation of proinsulin into newly synthesised ISG. Since the latter are preferentially released during regulated secretion [1–4], their reduced availability might contribute to the accompanying inhibition of GSIS in CREB2L2 depleted cells. The DEGs we identified using RNAseq, taken together with the RUSH analysis, suggest that CREB3L2 potentially impacts at multiple steps between the ER-export of proinsulin and its incorporation into ISGs. ER-to-Golgi trafficking was particularly highlighted by bioinformatic analysis, and confirmed at the protein level for Sec23a, which is a canonical target of CREB3L2 in other cell types [19,20]. We further demonstrated that loss of CREB3L2 exerted its greatest impact upstream of the condensation of proinsulin within the Golgi, consistent with a block in either ER-to-Golgi trafficking or intra-Golgi transit. In contrast, the absence of a Golgi stress signature amongst our DEGs, and the fact that distance distribution between the Golgi and newly synthesised ISGs was not altered by knockdown of CREB3L2, would argue against a major role in post-Golgi trafficking. Future studies will be required to confirm this, however, as well as to define the precise steps that CREB3L2 regulates upstream of proinsulin condensation.

CREDIT AUTHOR STATEMENT

Le May Thai: Data curation, Formal analysis, Investigation. **Atsushi Saito**: Methodology, Resources. **Mohammed Bensellam**: Investigation, Methodology, Writing — review & editing. **James Cantley**: Methodology, Supervision. **Nancy Sue**: Data curation, Formal analysis, Investigation, Methodology, Supervision, Writing — original draft. **Aimee Davenport**: Investigation, Methodology. **Jiang Tao**: Data curation, Methodology. **Fordham Ashleigh**: Formal analysis, Investigation. **Kazunori Imaizumi**: Conceptualization, Funding acquisition, Methodology, Resources, Supervision, Writing — review & editing. **Chenxu Yan**: Formal analysis, Investigation. **Trevor Biden**: Conceptualization, Formal analysis, Funding acquisition, Project administration, Supervision, Writing — original draft, Writing — review & editing. **Yan-Chuan Shi**: Investigation, Supervision. **Cierra Boyer**: Investigation, Methodology, Visualization. **Samuel Stephens**: Formal analysis, Methodology, Resources, Supervision, Writing — review & editing.

DATA AVAILABILITY

Data will be made available on request.

ACKNOWLEDGEMENTS

We are grateful for the expertise of the Australian Biological Resources and the Garvan Biological Testing Facility for mouse studes. We also thank staff of the Garvan Molecular Genetics Facility, the Kinghorn Centre for Clinical Genomics Sequencing Facilty, and the University of Iowa Viral Vector Core Facility. This work was supported by a Project Grant (1088390) and Research Fellowship (1024961) from the National Health and Medical Research Council of Australia to T.J.B, as well as grants from the Diabetes Australia Research Program (Y20G-BIDT) and the Garvan Research Foundation. There was also a Department of Defence Congressionally Directed Medical Research Program grant (W81XWH-20-1-0200) to S.B.S.

DECLARATION OF COMPETING INTEREST

The authors declare that they have no known competing financial interests or personal relationships that could have appeared to influence the work reported in this paper.

APPENDIX A. SUPPLEMENTARY DATA

Supplementary data to this article can be found online at https://doi.org/10.1016/j.molmet.2023.101845.

REFERENCES

[1] Boland BB, Rhodes CJ, Grimsby JS. The dynamic plasticity of insulin production in β-cells. Mol Metab 2017;6(9):958—73.
[2] Germanos M, Gao A, Taper M, Yau B, Kebede MA. Inside the insulin secretory granule. Metabolites 2021;11(8).
[3] Rohli KE, Boyer CK, Blom SE, Stephens SB. Nutrient regulation of pancreatic islet β-cell secretory capacity and insulin production. Biomolecules 2022;12(2).
[4] Vasiljevic J, Torkko JM, Knoch KP, Solimena M. The making of insulin in health and disease. Diabetologia 2020;63(10):1981—9.
[5] Skelly RH, Schuppin GT, Ishihara H, Oka Y, Rhodes CJ. Glucose-regulated translational control of proinsulin biosynthesis with that of the proinsulin endopeptidases PC2 and PC3 in the insulin-producing MIN6 cell line. Diabetes 1996;45(1):37—43.
[6] Ardestani A, Lupse B, Kido Y, Leibowitz G, Maedler K. mTORC1 signaling: a double-edged sword in diabetic β cells. Cell Metab 2018;27(2):314—31.
[7] Rutter GA, Leclerc I. The AMP-regulated kinase family: enigmatic targets for diabetes therapy. Mol Cell Endocrinol 2009;297(1—2):41—9.
[8] Durning SP, Flanagan-Steet H, Prasad N, Wells L. O-linked β-N-acetylglucosamine (O-GlcNAc) acts as a glucose sensor to epigenetically regulate the insulin gene in pancreatic beta cells. J Biol Chem 2016;291(5):2107—18.
[9] Hart GW. Nutrient regulation of signaling and transcription. J Biol Chem 2019;294(7):2211—31.
[10] Biden TJ, Boslem E, Chu KY, Sue N. Lipotoxic endoplasmic reticulum stress, β-cell failure and type 2 diabetes. Trends Endocrinol Metab 2014;25(8):389—98.
[11] Shrestha N, De Franco E, Arvan P, Cnop M. Pathological β-cell endoplasmic reticulum stress in type 2 diabetes: current evidence. Front Endocrinol (Lausanne) 2021;12:650158.
[12] Yong J, Johnson JD, Arvan P, Han J, Kaufman RJ. Therapeutic opportunities for pancreatic β-cell ER stress in diabetes mellitus. Nat Rev Endocrinol 2021;17(8):455—67.
[13] Cnop M, Toivonen S, Igoillo-Esteve M, Salpea P. Endoplasmic reticulum stress and eIF2α phosphorylation: the Achilles heel of pancreatic β cells. Mol Metab 2017;6(9):1024—39.
[14] Liu L, Cai J, Wang H, Liang X, Zhou Q, Ding C, et al. Coupling of COPII vesicle trafficking to nutrient availability by the IRE1α-XBP1s axis. Proc Natl Acad Sci U S A 2019;116(24):11776—85.
[15] Shaffer AL, Shapiro-Shelef M, Iwakoshi NN, Lee AH, Qian SB, Zhao H, et al. XBP1, downstream of Blimp-1, expands the secretory apparatus and other organelles, and increases protein synthesis in plasma cell differentiation. Immunity 2004;21(1):81—93.
[16] Kondo S, Saito A, Asada R, Kanemoto S, Imaizumi K. Physiological unfolded protein response regulated by OASIS family members, transmembrane bZIP transcription factors. IUBMB Life 2011;63(4):233—9.
[17] Kondo S, Hino SI, Saito A, Kanemoto S, Kawasaki N, Asada R, et al. Activation of OASIS family, ER stress transducers, is dependent on its stabilization. Cell Death Differ 2012;19(12):1939—49.
[18] Kondo S, Saito A, Hino S, Murakami T, Ogata M, Kanemoto S, et al. BBF2H7, a novel transmembrane bZIP transcription factor, is a new type of endoplasmic reticulum stress transducer. Mol Cell Biol 2007;27(5):1716—29.
[19] Khetchoumian K, Balsalobre A, Mayran A, Christian H, Chenard V, St-Pierre J, et al. Pituitary cell translation and secretory capacities are enhanced cell autonomously by the transcription factor Creb3l2. Nat Commun 2019;10(1):3960.
[20] Saito A, Hino S, Murakami T, Kanemoto S, Kondo S, Saitoh M, et al. Regulation of endoplasmic reticulum stress response by a BBF2H7-mediated Sec23a pathway is essential for chondrogenesis. Nat Cell Biol 2009;11(10):1197—204.
[21] Barrabi C, Zhang K, Liu M, Chen X. Pancreatic beta cell ER export in health and diabetes. Front Endocrinol (Lausanne) 2023;14:1155779.
[22] Lytrivi M, Ghaddar K, Lopes M, Rosengren V, Piron A, Yi X, et al. Combined transcriptome and proteome profiling of the pancreatic β-cell response to palmitate unveils key pathways of β-cell lipotoxicity. BMC Genomics 2020;21(1):590.
[23] Gu G, Dubauskaite J, Melton DA. Direct evidence for the pancreatic lineage: NGN3+ cells are islet progenitors and are distinct from duct progenitors. Development 2002;129(10):2447—57.
[24] Tamarina NA, Roe MW, Philipson L. Characterization of mice expressing Ins1 gene promoter driven CreERT recombinase for conditional gene deletion in pancreatic β-cells. Islets 2014;6(1):e27685.
[25] Chu KY, Mellet N, Thai LM, Meikle PJ, Biden TJ. Short-term inhibition of autophagy benefits pancreatic β-cells by augmenting ether lipids and

peroxisomal function, and by countering depletion of n-3 polyunsaturated fatty acids after fat-feeding. Mol Metab 2020:101023.

[26] Cantley J, Davenport A, Vetterli L, Nemes NJ, Whitworth PT, Boslem E, et al. Disruption of beta cell acetyl-CoA carboxylase-1 in mice impairs insulin secretion and beta cell mass. Diabetologia 2019;62(1):99–111.

[27] Cantley J, Burchfield JG, Pearson GL, Schmitz-Peiffer C, Leitges M, Biden TJ. Deletion of PKCε selectively enhances the amplifying pathways of glucose-stimulated insulin secretion via increased lipolysis in mouse β-cells. Diabetes 2009;58(8):1826–34.

[28] Miyazaki J, Araki K, Yamato E, Ikegami H, Asano T, Shibasaki Y, et al. Establishment of a pancreatic beta cell line that retains glucose-inducible insulin secretion: special reference to expression of glucose transporter isoforms. Endocrinology 1990;127(1):126–32.

[29] Busch AK, Cordery D, Denyer GS, Biden TJ. Expression profiling of palmitate- and oleate-regulated genes provides novel insights into the effects of chronic lipid exposure on pancreatic β-cell function. Diabetes 2002;51(4):977–87.

[30] Chu KY, O'Reilly L, Mellet N, Meikle PJ, Bartley C, Biden TJ. Oleate disrupts cAMP signaling, contributing to potent stimulation of pancreatic β-cell autophagy. J Biol Chem 2019;294(4):1218–29.

[31] Pearson GL, Mellet N, Chu KY, Cantley J, Davenport A, Bourbon P, et al. Lysosomal acid lipase and lipophagy are constitutive negative regulators of glucose-stimulated insulin secretion from pancreatic beta cells. Diabetologia 2014;57(1):129–39.

[32] Boyer CK, Bauchle CJ, Zhang J, Wang Y, Stephens SB. Synchronized proinsulin trafficking reveals delayed Golgi export accompanies β-cell secretory dysfunction in rodent models of hyperglycemia. Sci Rep 2023;13(1):5218.

[33] Bearrows SC, Bauchle CJ, Becker M, Haldeman JM, Swaminathan S, Stephens SB. Chromogranin B regulates early-stage insulin granule trafficking from the Golgi in pancreatic islet β-cells. J Cell Sci 2019;132(13).

[34] Karaskov E, Scott C, Zhang L, Teodoro T, Ravazzola M, Volchuk A. Chronic palmitate but not oleate exposure induces endoplasmic reticulum stress, which may contribute to INS-1 pancreatic β-cell apoptosis. Endocrinology 2006;147:3398–407.

[35] Kharroubi I, Ladriere L, Cardozo AK, Dogusan Z, Cnop M, Eizirik DL. Free fatty acids and cytokines induce pancreatic β-cell apoptosis by different mechanisms: role of nuclear factor-kB and endoplasmic reticulum stress. Endocrinology 2004;145(11):5087–96.

[36] Laybutt DR, Preston AM, Akerfeldt MC, Kench JG, Busch AK, Biankin AV, et al. Endoplasmic reticulum stress contributes to beta cell apoptosis in type 2 diabetes. Diabetologia 2007;50(4):752–63.

[37] Elouil H, Bensellam M, Guiot Y, Vander Mierde D, Pascal SM, Schuit FC, et al. Acute nutrient regulation of the unfolded protein response and integrated stress response in cultured rat pancreatic islets. Diabetologia 2007;50(7):1442–52.

[38] Greenman IC, Gomez E, Moore CE, Herbert TP. Distinct glucose-dependent stress responses revealed by translational profiling in pancreatic β-cells. J Endocrinol 2007;192(1):179–87.

[39] Sharma RB, O'Donnell AC, Stamateris RE, Ha B, McCloskey KM, Reynolds PR, et al. Insulin demand regulates β cell number via the unfolded protein response. J Clin Invest 2015;125(10):3831–46.

[40] Henquin JC, Nenquin M, Stiernet P, Ahren B. In vivo and in vitro glucose-induced biphasic insulin secretion in the mouse: pattern and role of cytoplasmic Ca2+ and amplification signals in beta-cells. Diabetes 2006;55(2):441–51.

[41] Ma J, Wu C, Hart GW. Analytical and biochemical perspectives of protein O-GlcNAcylation. Chem Rev 2021;121(3):1513–81.

[42] Fan J, Wang Y, Liu L, Zhang H, Zhang F, Shi L, et al. cTAGE5 deletion in pancreatic β cells impairs proinsulin trafficking and insulin biogenesis in mice. J Cell Biol 2017;216(12):4153–64.

[43] Lekszas C, Foresti O, Raote I, Liedtke D, Konig EM, Nanda I, et al. Biallelic TANGO1 mutations cause a novel syndromal disease due to hampered cellular collagen secretion. Elife 2020;9.

[44] Saegusa K, Matsunaga K, Maeda M, Saito K, Izumi T, Sato K. Cargo receptor Surf4 regulates endoplasmic reticulum export of proinsulin in pancreatic β-cells. Commun Biol 2022;5(1):458.

[45] Wang L, Liu H, Zhang X, Song E, Wang Y, Xu T, et al. WFS1 functions in ER export of vesicular cargo proteins in pancreatic β-cells. Nat Commun 2021;12(1):6996.

[46] Bensellam M, Van Lommel L, Overbergh L, Schuit FC, Jonas JC. Cluster analysis of rat pancreatic islet gene mRNA levels after culture in low-, intermediate- and high-glucose concentrations. Diabetologia 2009;52(3):463–76.

[47] Fang Z, Weng C, Li H, Tao R, Mai W, Liu X, et al. Single-cell heterogeneity analysis and CRISPR screen identify key beta-cell-specific disease genes. Cell Rep 2019;26(11):3132–3144 e3137.

[48] De Franco E, Lytrivi M, Ibrahim H, Montaser H, Wakeling MN, Fantuzzi F, et al. YIPF5 mutations cause neonatal diabetes and microcephaly through endoplasmic reticulum stress. J Clin Invest 2020;130(12):6338–53.

[49] Yang J, Zhen J, Feng W, Fan Z, Ding L, Yang X, et al. IER3IP1 is critical for maintaining glucose homeostasis through regulating the endoplasmic reticulum function and survival of β cells. Proc Natl Acad Sci U S A 2022;119(45):e2204443119.

[50] Bone RN, Oyebamiji O, Talware S, Selvaraj S, Krishnan P, Syed F, et al. A computational approach for defining a signature of β-cell Golgi stress in diabetes. Diabetes 2020;69(11):2364–76.

[51] El Ouaamari A, Zhou JY, Liew CW, Shirakawa J, Dirice E, Gedeon N, et al. Compensatory islet response to insulin resistance revealed by quantitative proteomics. J Proteome Res 2015;14(8):3111–22.

[52] Osipovich AB, Stancill JS, Cartailler JP, Dudek KD, Magnuson MA. Excitotoxicity and overnutrition additively impair metabolic function and identity of pancreatic β-cells. Diabetes 2020;69(7):1476–91.

[53] Parchure A, Tian M, Stalder D, Boyer CK, Bearrows SC, Rohli KE, et al. Liquid-liquid phase separation facilitates the biogenesis of secretory storage granules. J Cell Biol 2022;221(12).

[54] Hassler JR, Scheuner DL, Wang S, Han J, Kodali VK, Li P, et al. The IRE1α/XBP1s pathway is essential for the glucose response and protection of β cells. PLoS Biol 2015;13(10):e1002277.

[55] Lee K, Chan JY, Liang C, Ip CK, Shi YC, Herzog H, et al. XBP1 maintains beta cell identity, represses beta-to-alpha cell transdifferentiation and protects against diabetic beta cell failure during metabolic stress in mice. Diabetologia 2022;65(6):984–96.

[56] Lipson KL, Fonseca SG, Ishigaki S, Nguyen LX, Foss E, Bortell R, et al. Regulation of insulin biosynthesis in pancreatic beta cells by an endoplasmic reticulum-resident protein kinase IRE1. Cell Metab 2006;4(3):245–54.

[57] Preston AM, Gurisik E, Bartley C, Laybutt DR, Biden TJ. Reduced endoplasmic reticulum (ER)-to-Golgi protein trafficking contributes to ER stress in lipotoxic mouse beta cells by promoting protein overload. Diabetologia 2009;52(11):2369–73.

[58] Boslem E, MacIntosh G, Preston AM, Bartley C, Busch AK, Fuller M, et al. A lipidomic screen of palmitate-treated MIN6 β-cells links sphingolipid metabolites with endoplasmic reticulum (ER) stress and impaired protein trafficking. Biochem J 2011;435(1):267–76.

[59] Boslem E, Weir JM, Macintosh G, Sue N, Cantley J, Meikle PJ, et al. Alteration of endoplasmic reticulum lipid rafts contributes to lipotoxicity in pancreatic β-cells. J Biol Chem 2013;288:26569–82.

[60] Vander Mierde D, Scheuner D, Quintens R, Patel R, Song B, Tsukamoto K, et al. Glucose activates a protein phosphatase-1-mediated signaling pathway

to enhance overall translation in pancreatic β-cells. Endocrinology 2007; 148(2):609–17.
[61] Shrestha S, Erikson G, Lyon J, Spigelman AF, Bautista A, Manning Fox JE, et al. Aging compromises human islet beta cell function and identity by decreasing transcription factor activity and inducing ER stress. Sci Adv 2022;8(40):eabo3932.
[62] Gomez E, Powell ML, Greenman IC, Herbert TP. Glucose-stimulated protein synthesis in pancreatic β-cells parallels an increase in the availability of the translational ternary complex (eIF2-GTP.Met-tRNAi) and the dephosphorylation of eIF2 alpha. J Biol Chem 2004;279(52):53937–46.
[63] Konrad RJ, Kudlow JE. The role of O-linked protein glycosylation in β-cell dysfunction. Int J Mol Med 2002;10(5):535–9.
[64] Alejandro EU, Bozadjieva N, Kumusoglu D, Abdulhamid S, Levine H, Haataja L, et al. Disruption of O-linked N-acetylglucosamine signaling induces ER stress and β cell failure. Cell Rep 2015;13(11):2527–38.
[65] Lockridge A, Jo S, Gustafson E, Damberg N, Mohan R, Olson M, et al. Islet O-GlcNAcylation is required for lipid Potentiation of insulin secretion through SERCA2. Cell Rep 2020;31(5):107609.
[66] Lewis CA, Griffiths B, Santos CR, Pende M, Schulze A. Regulation of the SREBP transcription factors by mTORC1. Biochem Soc Trans 2011;39(2): 495–9.
[67] Adegoke OAJ, Beatty BE, Kimball SR, Wing SS. Interactions of the super complexes: when mTORC1 meets the proteasome. Int J Biochem Cell Biol 2019;117:105638.
[68] Sampieri L, Funes Chaban M, Di Giusto P, Rozes-Salvador V, Alvarez C. CREB3L2 modulates nerve growth factor-induced cell differentiation. Front Mol Neurosci 2021;14:650338.
[69] Cunha DA, Ladriere L, Ortis F, Igoillo-Esteve M, Gurzov EN, Lupi R, et al. Glucagon-like peptide-1 agonists protect pancreatic β-cells from lipotoxic endoplasmic reticulum stress through upregulation of BiP and JunB. Diabetes 2009;58(12):2851–62.
[70] Yusta B, Baggio LL, Estall JL, Koehler JA, Holland DP, Li H, et al. GLP-1 receptor activation improves β cell function and survival following induction of endoplasmic reticulum stress. Cell Metab 2006;4(5):391–406.
[71] Bensellam M, Maxwell EL, Chan JY, Luzuriaga J, West PK, Jonas JC, et al. Hypoxia reduces ER-to-Golgi protein trafficking and increases cell death by inhibiting the adaptive unfolded protein response in mouse beta cells. Diabetologia 2016;59(7):1492–502.
[72] Ishikura-Kinoshita S, Saeki H, Tsuji-Naito K. BBF2H7-mediated Sec23A pathway is required for endoplasmic reticulum-to-Golgi trafficking in dermal fibroblasts to promote collagen synthesis. J Invest Dermatol 2012;132(8):2010–8.
[73] Tomoishi S, Fukushima S, Shinohara K, Katada T, Saito K. CREB3L2-mediated expression of Sec23A/Sec24D is involved in hepatic stellate cell activation through ER-Golgi transport. Sci Rep 2017;7(1):7992.
[74] Gupta D, Jetton TL, LaRock K, Monga N, Satish B, Lausier J, et al. Temporal characterization of β cell-adaptive and -maladaptive mechanisms during chronic high-fat feeding in C57BL/6NTac mice. J Biol Chem 2017;292(30):12449–59.
[75] Huang H, Yang K, Wang R, Han WH, Kuny S, Zelmanovitz PH, et al. β-Cell compensation concomitant with adaptive endoplasmic reticulum stress and beta-cell neogenesis in a diet-induced type 2 diabetes model. Appl Physiol Nutr Metab 2019;44(12):1355–66.
[76] Kahn SE, Zraika S, Utzschneider KM, Hull RL. The beta cell lesion in type 2 diabetes: there has to be a primary functional abnormality. Diabetologia 2009;52(6):1003–12.

